Design and Integration of a Novel Robotic Leg Mechanism for Dynamic Locomotion at High-Speeds

Vinaykarthik R. Kamidi

Thesis submitted to the Faculty of the
Virginia Polytechnic Institute and State University
in partial fulfillment of the requirements for the degree of

Masters of Science
in
Mechanical Engineering

Pinhas Ben-Tzvi, Chair
Alexander Leonessa
Tomonari Furukawa

December 19, 2017
Blacksburg, Virginia

Keywords: Legged Locomotion , Mechanism & Design

Design and Integration of a Novel Robotic Leg Mechanism for Dynamic Locomotion at High-Speeds

Vinaykarthik R. Kamidi

ABSTRACT

Existing state-of-the-art legged robots often require complex mechanisms with multi-level controllers and computationally expensive algorithms. Part of this is owed to the multiple degrees of freedom (DOFs) these intricate mechanisms possess and the other is a result of the complex nature of dynamic legged locomotion. The underlying dynamics of this class of non-linear systems must be addressed in order to develop systems that perform natural human/animal-like locomotion. However, there are no stringent rules for the number of DOFs in a system; this is merely a matter of the locomotion requirements of the system. In general, most systems designed for dynamic locomotion consist of multiple actuators per leg to address the balance and locomotion tasks simultaneously.

In contrast, this research hypothesizes the decoupling of locomotion and balance by omitting the DOFs whose primary purpose is dynamic disturbance rejection to enable a far simplified mechanical design for the legged system. This thesis presents a novel single DOF mechanism that is topologically arranged to execute a trajectory conducive to dynamic locomotive gaits. To simplify the problem of dynamic balancing, the mechanism is designed to be utilized in a quadrupedal platform in the future. The preliminary design, based upon heuristic link lengths, is presented and subjected to kinematic analysis to evaluate the resulting trajectory. To improve the result and to analyze the effect of key link lengths, sensitivity analysis is then performed. Further, a reference trajectory is established and a parametric optimization over the design space is performed to drive the system to an optimal configuration.

The evolved design is identified as the Bio-Inspired One-DOF Leg for Trotting (BOLT). The

dynamics of this closed kinematic chain mechanism is then simplified, resulting in a minimal order state space representation. A prototype of the robotic leg was integrated and mounted on a treadmill rig to perform various experiments. Finally, open loop running is implemented on the integrated prototype demonstrating the locomotive performance of BOLT.

Design and Integration of a Novel Robotic Leg Mechanism for Dynamic Locomotion at High-Speeds

Vinaykarthik R. Kamidi

GENERAL AUDIENCE ABSTRACT

Existing state-of-the-art legged robots often require complex mechanisms with multi-level controllers and computationally expensive algorithms. Part of this is owed to the multiple degrees of freedom (DOFs) these intricate mechanisms possess and the other is a result of the complex nature of dynamic legged locomotion. The underlying dynamics of this class of non-linear systems must be addressed in order to develop systems that perform natural human/animal-like locomotion. However, the number of active DOF is merely a designers choice.

To simplify the problem at both levels: design and controls of dynamic locomotion, we developed a novel mechanism that incorporates the benefits of higher DOF legs while accommodating the simplicity of single DOF leg. The preliminary design of the mechanism was designed with parameters (lengths of the femur,tibia) that were directly derived from a domestic dog.

Synthesis of the mechanism suggested that the design was not suitable for an intended running-trot gait observed in biological counterparts. However, to gain a deeper understanding of the mechanism, it was necessary to perform a sensitivity analysis, as a result we arrived at a mechanism whose performance was better than the initial but still not satisfactory.With the insight gained through the analysis and an ideal gait design exercise, then an optimization on the design space was performed with carefully tuned bounds. The final result is a novel mechanism identified as Biologically inspired One DOF Leg for Trotting (BOLT) that is topologically arranged to execute a running-trot gait.

Finally, the design choice presented with a challenge that has not been actively addressed. The dynamics of the mechanism can not be modeled using traditional methods due to presence of constraints that characterize the closed loops of the mechanism. We present an adaption of the Singularly perturbed dynamic model for systems that are hybrid in nature. The resulting dynamics are simplified, resulting in a minimal order state space representation, which is more amenable to model based control development in future. A prototype of the robotic leg was integrated and mounted on a treadmill rig to perform various experiments.Finally, open loop running is implemented on the integrated prototype demonstrating the locomotive performance of BOLT.

Acknowledgments

First and foremost, I would like to thank my parents, Laxma Reddy and Aruna, for the love and unrelenting support. Without your encouragement I would not have made it through.

Thank you to my advisor, Dr. Pinhas Ben-Tzvi, who has provided me invaluable support and guidance throughout my graduate career. I appreciate the opportunities you have provide me, and the unhesitating willingness to provide help.

Thank you to Peter Racioppo, Adam Williams, Anil Kumar, Bijo Sebastien and Will Rone. Your feedback and direction paved the way to my research. I appreciate your friendship and advice.

I would also like to thank my extended family and friends for all their support.

Contents

1 Introduction **1**

1.1 Motivation For Study of Robotic Legs 1

1.2 State of the Art Legged robots 2

1.2.1 High-Speed Legged Locomotion 3

1.2.2 Reduced Degree of Freedom Leg design 5

1.2.3 Control framework 7

1.3 Structure of the thesis 8

1.4 Attribution 9

1.5 Contributions 9

1.6 Selected Publications 10

2 Mechanism Design and Synthesis **11**

2.1 Design Motivation and Objectives 11

2.2 Preliminary Design 12

2.3 Kinematic Analysis 13

2.3.1 Preliminaries 14

2.3.2 Multibody Method (Iterative Solution) 15

2.4 Ideal Stride-phase Trajectory Design 17

2.5 Sensitivity Analysis 18

2.6 Comparison Metrics 22

2.7 Discussion 24

3 Design and Optimization **26**

3.1 Design Evolution 26

3.1.1 Objective function 27

3.2 Kinematic mapping 28

3.2.1 Vector loop method 29

3.2.2 Results 32

3.3 Robotic leg Design 34

4 Single Leg Dynamics of BOLT **37**

4.1 Mathematical description 38

4.1.1 Underlying Equations of Motion 40

4.1.2 Singularly Perturbed Formulation (SPF) 42

5 Experimental validation **45**

5.1 Experimental Setup 45

5.2 Trajectory Validation experiment 46

5.3 Open loop running 47

6 Conclusion & Future Work **49**

6.1 Summary 49

6.2 Future Work 50

Bibliography **53**

A Floating Base EOM utilizing SPF **61**

List of Figures

1.1 State of the art legged robots top left: mini spot top right: HYQ2 bottom left: ETH StarlETH bottom right: MIT cheetah 2 3

1.2 Existing high-speed legs: (a) MIT cheetah leg (b) Hydraulic leg of HYQ robot, IIT (c) Boston dynamics Cheetah 4

1.3 Existing Single Degree of Freedom mechanisms: (A) Jansen Linkage, (B) Ghassei Linkage, (C) Klann Mechanism, (D) Watt-I (E) Stephenson-II, (F) Stephenson-III 6

2.1 CAD rendering of the preliminary design with link lengths chosen by heuristics 13

2.2 Kinematic scheme adopted for the initial design of the mechanism. Shown in the inset are the generated trajectories. 15

2.3 Designed trajectory 17

2.4 Bounded sensitivity analysis: (a) Crank shaft vs Stride length (b) Hip-crank distance vs Angle of attack 20

2.5 Plot showing the effects of varying link lengths L_1 21

2.6 Plot showing the effects of varying link lengths L_6 22

2.7 Realization of the best trajectory from the simulated trajectories. 24

3.1 Kinematic model used for the vector-loop analysis 30

3.2 Illustration of kinematic equivalence after performing vector loop analysis . . 32

3.3 a)illustrating the optimized leg executing the optimized trajectory. (b) Trajectory executed by the mechanism prior and after optimization (c) Close up view of the optimized trajectory 33
3.4 3D rendering of the optimized Leg (BOLT) 34
3.5 Angular displacements before and after optimization 36

4.1 Illustrating the virtual separation method adopted to alleviate modeling of CKC mechanism on the left. Towards the right the rejoining is performed once the reduced order state space model is achieved. 40
4.2 Schematic model of BOLT denoting the nomenclature used to derive the dynamic description. 41

5.1 Setup for testing BOLTs running gait: 1) BOLT, 2) Higher level controller, 3) Low-level controller, 4) LiPo batteries in series, 5) Emergency stop, 6) Treadmill. 45
5.2 Illustrating the executed trajectory (red) by BOLT. (a)Depiction of the estimated trajectory at the speed of 1m/s. (b) Comparison of the designed trotting trajectory vs estimated trajectory at 3.2 m/s. 47
5.3 Timestamps illustrating one step cycle of the BOLT in open loop control . . 48

6.1 CAD rendering of the quadruped with the proposed leg mechanism 51
6.2 Fusion of the tail with the quadruped 52

List of Tables

1.1 Comparison table of notable existing robots against the proposed mechanism (BOLT) 7

2.1 Control points utilized in the bezier cure formulation 18

2.2 Hausdorff distances of the simulated trajectories 23

2.3 Jaccard distances of the simulated trajectories. 23

3.1 Optimized Design Variables 28

Chapter 1

Introduction

1.1 Motivation For Study of Robotic Legs

Legged locomotion has shown potential benefits in traversing uneven terrain and obstacles in comparison to wheeled and tracked vehicles [1]. Only a few robots have been successfully implemented in real-world applications due to relative complexity of design and control of legged machines. Such examples include, but are not limited to, the ANYmal quadruped [2] and the Adaptive Suspension Vehicle [3] developed for nuclear power plant maintenance and field transportation, respectively. Considerable research was devoted to the investigation of dynamic stability control [4], and walking pattern generation [5]. However, the leg mechanism determines the number of active DOF required for operation. This corresponds to the efficiency of the system, thus making these components fundamental for the design and operational aspects of legged robots as pointed out in [6]. For a legged robot to navigate utilizing a symmetric or asymmetric gait, perform forward motion, and turning maneuvers on uneven terrain, a minimum of three active DOFs are required for spatial positioning. Turning is often the least used motion during walking/trotting gaits. Traditionally the hip Abduction/

Adduction (HAA) DOF is responsible for turning and is separated from the other two-DOFs, hip Extension/Flexion (HFE) and knee Extension/Flexion (KFE). Typically, two DOF leg designs [7] are sufficient to engage HFE and KFE to locomote dynamically in a plane. However, multiple actuators are required to change direction cyclically during a walking/trotting gait.

In addition, both DOFs must be controlled simultaneously, which results in complex control algorithms and slow speed, static gaits when implemented either on bipedal/quadrupedal robots.To address these challenges, the authors present a novel single-DOF leg conducive to performing a dynamic gait, namely trotting/running-trot at high speeds when mounted on a quadrupedal platform. This paper investigates the hypothesis that leg mechanisms designed with reduced DOFs can trace a foot trajectory favorable to dynamic locomotion.

The long-term goal of this research is to develop a quadrupedal robot capable of performing high-speed, planar trot-running. The fully integrated quadruped will be used as an experimental platform to investigate the benefits of stabilization and maneuvering of legged robots using articulated spatial robotic tails [8] [9] [10] [11] .

1.2 State of the Art Legged robots

This section gives an overview of applicable research about design and control of legged robots, particularly quadrupedal robotic systems with the focus on recent achievements and research results that directly impacted our approach.

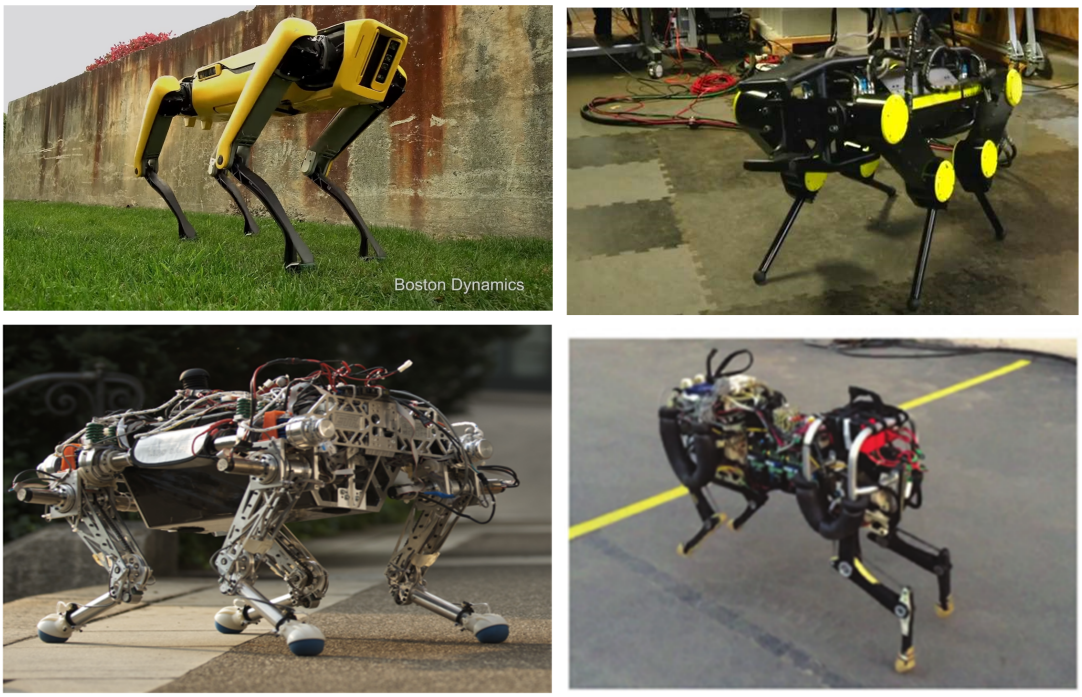

Figure 1.1: State of the art legged robots top left: mini spot top right: HYQ2 bottom left: ETH StarlETH bottom right: MIT cheetah 2

1.2.1 High-Speed Legged Locomotion

This section reviews high-speed legged robots with emphasis on their design topologies, active DOFs, gait types and the demonstrated forward velocities of the legged robotic platform. Observations from nature indicate that fast locomotion can be realized by asymmetric gaits such as trotting and bounding [12]. These gaits are referred to as dynamic gaits due to the requirement of active balancing while in motion. The step cycles involved in these motions may be divided into two stages: the stance phase, in which the foot contacts the ground, absorbs impact forces, and pushes the robot forward, and the swing phase, in which the leg is moved to a new contact point.

The MIT Cheetah Quadruped, shown in Figure 1.2a (a), utilizes legs with two active DOFs and custom designed actuators located at the hip and shoulder joints and has demonstrated trotting speeds of 6 m/s [13]. It employs virtual compliance between the hip and the distal

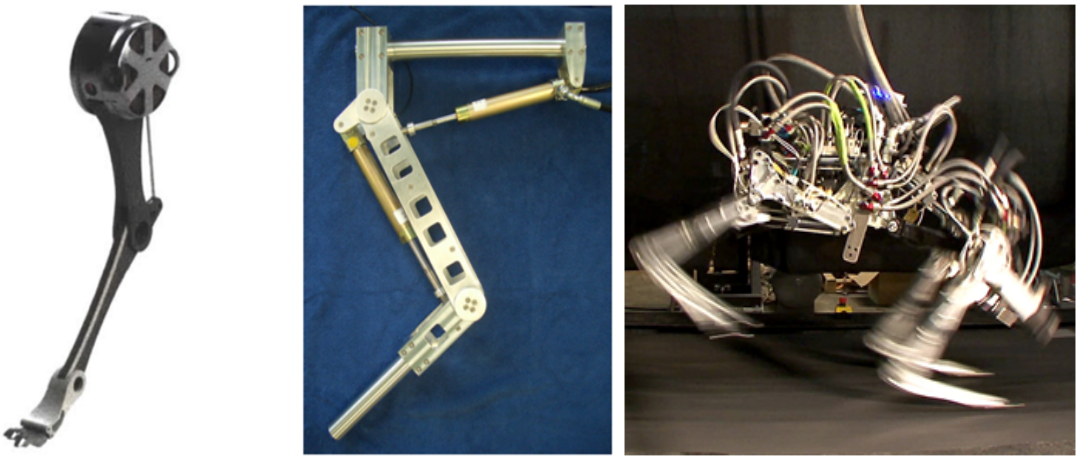

(a) (b) (c)

Figure 1.2: Existing high-speed legs: (a) MIT cheetah leg (b) Hydraulic leg of HYQ robot, IIT (c) Boston dynamics Cheetah

link of its three-link leg structure, where a multi-layered controller is used to shield the motors from impact forces [14]. The HYQ, a hydraulically and electrically actuated quadruped, shown in **??** (b), employs legs with three active DOFs each and has exhibited trotting at speeds up to 2.2 m/s [15]. It utilizes a two-link leg similar in structure to that of plantigrades, and employed a high-level controller to plan its leg trajectory [16]. The KAIST robot, illustrated in Figure 1.2b, is a bipedal platform that runs at an average speed of 0.75 m/s, with a step frequency of 2.8 HZ [17]. Its motors are also located at the hip and it uses a physical spring positioned in the distal part of the leg to absorb impact forces experienced at the foot in dynamic locomotion. Figure 1.2c shows the Boston Dynamics Cheetah, which reported a maximum attainable speed on a treadmill of 12.9 m/s using an off-board hydraulic unit with its digitigrade leg structure.

As the above discussion demonstrates, in platforms employing electric actuation and tetherless locomotion it is preferable to locate motors close to the hip, so that the reflected inertia at the distal part of the legs is reduced, and higher speeds can be achieved. It also worth noting that compliance within the leg mechanism, physical or virtual, is necessary to absorb

the impact forces of high-speed locomotion. However, the majority of legs in the literature have to synchronize multiple actuators and employ a multi- layered control structure in order to execute the required trajectory. In addition, the integration of multiple active DOF joints correlate to a greater mass and bulkier structures requiring more power from the motors to locomote.

1.2.2 Reduced Degree of Freedom Leg design

To address the challenges of highly articulated leg design, researchers have investigated reduced-DOF strategies. In this paper, a reduced-DOF legged system is defined as one possessing one or two active DOFs. The RMLeg is a two- DOF leg composed of two four-bar mechanisms in an arrangement designed to produce a stable walking gait [7]. The design requires two motors working in tandem to generate one step cycle, resulting in low efficiency, as its reported speed of 0.1 m/s reflects. The Rhex robot utilizes six C-shaped legs, each independently actuated and capable of continuous rotation about a motor shaft [17]. The robot successfully implemented a pronking gait at 0.55 m/s. A variety of single-DOF leg mechanisms, such as those depicted in Fig. 2, have been explored in previous research [18]. Analysis of reported trajectories shows that these mechanisms produce approximately straight-line stance phase trajectories. The Jansen mechanism depicted in Figure 1.3 (A), the Ghassei linkage in Figure 1.3 (B), and the Klann linkage, as shown in Figure 1.3(C), are all crank-based leg mechanisms that exhibit straight-line approximations [19]. Many of the trajectories that can be created by the Watt-I mechanism in Figure 1.3 (D), and the Stephenson-II and Stephenson-III mechanisms in Figure 1.3 (E) and Figure 1.3 (F) respectively, have complicated swing phases that require the leg to trace complicated curves or suddenly transition into protraction, resulting in undesirable sharp turns. Prior analysis shows that the stance-phase trajectory for fast locomotion is dictated by the minimum amount of

time the leg is in contact with the ground, as is exhibited by the sinusoidal wave observations made in [20]. Simple mechanisms with reduced DOFs may be constructed, which have lower mass, cost, and control requirements than legs with three or more DOFs. The drawback of these designs is that they limit the achievable workspace of the leg, thus making it difficult to maintain stability while executing dynamic gaits or maneuvers. Reduced-DOF legs typically compensate for their reduced workspace by employing static gaits, redundant structures, or lower speed walking gaits. However,reduced-DOF mechanisms must also deal with the problem of motor synchronization. Additionally, running at high speeds is more efficient if actuators are not required to change direction during a step cycle. In summary, while reduced- DOF mechanisms are a promising means of reducing the design and control com-

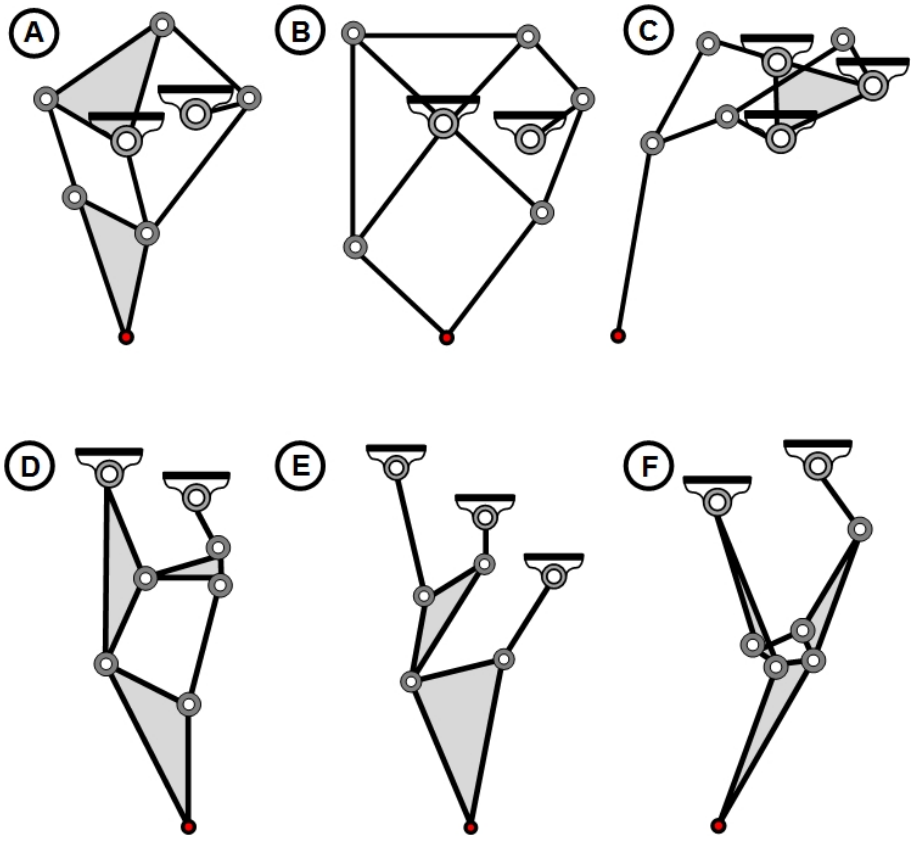

Figure 1.3: Existing Single Degree of Freedom mechanisms: (A) Jansen Linkage, (B) Ghassei Linkage, (C) Klann Mechanism, (D) Watt-I (E) Stephenson-II, (F) Stephenson-III

Table 1.1: Comparison table of notable existing robots against the proposed mechanism (BOLT)

Robot	Mechanism	DOF	Locomotion	Speed(m/s)
MIT Cheetah	Serial chain	3	Dynamic locomotion	6
HYQ	Serial chain	3	Dynamic locomotion	2.1
StarlETH	Serial chain	3	Dynamic locomotion	0.7
RM leg	close chain	2	Quasi-static locomotion	0.1
Minitaur Leg	closed chain	2	Dynamic locomotion	2
SCOUT-II	Prismatic leg	1	Dynamic locomotion	1.2
KAIST Raptor	8-bar closed chain	1	Dynamic locomotion	12.7
BOLT	**6-bar closed chain**	**1**	**Dynamic Locomotion**	**3.2**

plexity involved in leg locomotion, the problems of minimizing ground contact, synchronizing motor actuation, and optimizing distal mass distribution in such systems remain a research challenge. An overview of the existing legged robots against the proposed mechanism is given in Table 1.1

1.2.3 Control framework

The above highlighted robots have hierarchical complex control architectures that are coordinated to be able to take a single step[21],[14],[22]. Usually, they are broken down into high-level and low-level controllers. Compositionally, the higher level controllers includes gait sequencing strategies, whole-body trajectory generators [23]. while then the lower-level controllers would comprise (i) a foot trajectory generator that respects the whole body trajectory generated by the higher-level controller. (ii) an inverse kinematic controller then plans the leg motion with respect to the generated foot trajectory all while avoiding sin-

gularities [24]. In particular the robustness of the low-level controller is still being worked [25],[26],[27] to account for delays, singularities before these robots are navigating the urban environments.

An alternative approach that has shown promise in quadrupedal platforms is the implementation of only one actuator per leg as seen in [28].However, the prismatic leg design of Scout-II is an oversimplification that results in robotic-like bounding. Therefore the need for a mechanism that combines the performance of multi-DOF legs with the simplicity of the one-DOF legs is identified and the prime motivator for this work.

1.3 Structure of the thesis

This thesis is organized in the following format.

Chapter 2 presents the conception of the mechanism and the kinematic model of preliminary design using multibody dynamics methods. It also establishes an ideal trajectory that is conducive to dynamic locomotive gaits. Further it details the sensitivity analysis undertaken to identify the effect of various link lengths on the foot trajectory. Results and discussion follows.

Chapter 3 builds on the lessons learned from the sensitivity analysis in Chapter 2, parametric optimization is performed on the first design to arrive at a better design that satisfies our requirements. A Kinematic model of the evolved design is developed, but utilizing vector loop methods to partly reduce computation burden for real-time implementation in future.

Chapter 4 describes the dynamics of the BOLT leg. Since, the mechanism is a closed Kinematic chain mechanism (CKC), first methods are explored to substitute the Algebraic equations with an approximate ODE. Then, a novel implementation of the singularly per-

turbed formulation for floating base dynamics is presented.

Chapter 5 details the experiments performed and analyses the corresponding results. Open loop running experiments are performed on the integrated platform and the capabilities of the mechanism are elucidated.

Chapter 6 Concludes this thesis and provides a summary of this work and the future direction of the research

1.4 Attribution

Chapter 2 is an expansion of the contents published in the 2017 IEEE International Conference on Intelligent Robots and Systems (IROS)[29]. Wael Saab performed a literature survey of the existing work. Pinhas Ben-Tzvi then provided insights that steered the manuscript in to the right direction.

1.5 Contributions

The proposed contributions of this thesis are as follows:

1. Development of a novel one DOF robotic leg mechanism conducive to dynamic locomotive gaits.

2. Inclusion of Parametric optimization of the mechanism to better match the leg trajectory to the trot gaits observed in animals.

3. Derivation of floating base dynamics of CKC mechanisms using SP formulation.

1.6 Selected Publications

This work has resulted in the following papers, and were either presented at conferences,or are in progress. Note that these papers form the structure of this thesis.

- Vinay Kamidi, wael saab, and Pinhas Ben-Tzvi,"Design and Analysis of a Novel Planar Robotic Leg for High-Speed Locomotion".In: *IEEE/RSJ International Conference on Intelligent Robots and Systems (IROS).* September 2017.

- Vinay Kamidi and Pinhas Ben-Tzvi,"Proprioceptive Control for Accurate Foothold Placement Aiding Fast-Legged Locomotion". In: *Transaction of Robotics.* In progress

In addition the following poster was also presented.

- Kamidi, V., Ben-Tzvi, P., Experimental Validation of Dynamic Legged Locomotion Utilizing a Single-DOF Robotic Leg, *Proceedings of the 2017 IEEE/RSJ International Conference on Intelligent Robots and Systems (IROS2017)*, Vancouver, Canada, Sep. 24 - 28, 2017.

Chapter 2

Mechanism Design and Synthesis

2.1 Design Motivation and Objectives

It is desirable for a legged robot to have an efficient control structure and a simple mechanical structure while at the same time being capable of locomoting at high-speeds. Furthermore, fast running is a function of both the actuation and the physical characteristics of the leg mechanism. Exploiting the properties of single-DOF mechanisms removes the need for synchronized motor control within the leg. As stated previously, minimization of the distal mass of the mechanism transfers the legs inertial moment closer to the body, thus increasing achievable speed. In addition, the trajectory must be smooth in order minimize ground contact, thus increasing the force generated with each step to propel forward. The angle of attack (the angle at which the leg approaches the ground) plays a crucial role in stable running. Therefore, it has to be kept to a minimum as established in.[30] Finally, the desire for a compact and robust mechanism is to reduce the required actuation power while still enabling it to withstand the high impact motion of running.

Therefore, the objective of this research is summarized according to the following require-

ments for the leg to satisfy:

- The leg mechanism should only be driven by a single, continuously rotating link.
- The mechanism should be designed with reduced inertia for high-speed applications.
- The generated foot trajectory should be a smooth closed loop curve.
- The angle of attack should be minimized.
- The mechanism should be compact and robust.

2.2 Preliminary Design

This section details the mechanical design of the proposed leg mechanism, illustrated in a schematic diagram shown in Fig. 3. The leg is a six-bar mechanism, with its five links denoted as the femur, tibia, HFE link, KFE link, and the driver link, responsible for actuation.
The driver is attached to a high power geared motor and is capable of continuous rotation. Motion is transferred to the femur and tibia links via the HFE and KFE linkages resulting in a closed loop, smooth foot trajectory, a sample of which is shown in Figure Figure 2.2 This mechanical arrangement fulfills Requirement 1. The hip and the driver are located close to each other on the body, at an offset, with the driver placed close to the hip to satisfy Requirement 2.
In order to dissipate energy resulting from impact during a high-speed gait, a spring damper system is incorporated into a translational joint located at the end of the tibia that represents the foot. A linear potentiometer provides a means of measuring the displacement of the spring that corresponds to a force feedback signal that can be used to compute stability

criterion. A conceptual quadrupedal model with the designed legs is illustrated in Figure 2.1.

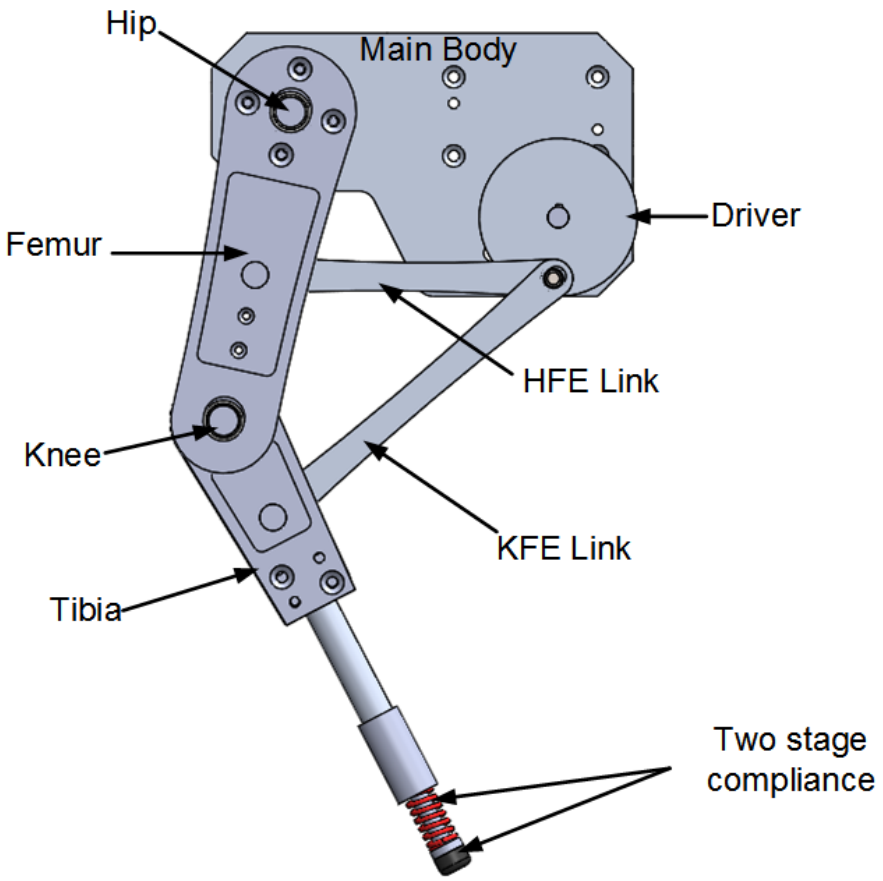

Figure 2.1: CAD rendering of the preliminary design with link lengths chosen by heuristics

2.3 Kinematic Analysis

This section presents the kinematic analysis performed to estimate the foot position, using a multibody formulation.

2.3.1 Preliminaries

In order to model a planar mechanism, first a global co-ordinate frame is defined as $[x, y]^T$. Further, for body i a body-fixed reference frame, $[x'_i, y'_i]^T$ is designated. Note that the body-fixed frame is interchangeably refereed to as local-frame. Additionally the orientation of this body with respect to the global frame is given by ϕ_i. Then the position of body i in the global frame can be given by $\boldsymbol{r_i}$. Thereafter, any point, P_i in the body can be pinpointed by a vector s_i^P in the global frame. Conveniently, position in the local frame can be given after a angle transformation by vector s'^P_i. With the notational dependencies established, it becomes easier to understand the constraint definitions this framework entails.

The mechanism under analysis contains driving, distance and revolute constraints. Hence, in this thesis only these equations are divulged. The distance constraint is given as some function of time as in Equation 2.1

$$\Phi^D(t) = f(t) \tag{2.1}$$

To define the revolute constraint, consider two bodies i and j. By definition,the revolute joint results from the juxtaposition of point P_i on body i and point $p_j$on body j, i.e the distance between p_i and $p_j$is zero which is mathematically translated in the global frame as Equation 2.2

$$d_{ij} = r_j + s_j^P - r_i - s_i^P = 0 \tag{2.2}$$

with the distance constraint defined, the revolute joint is therefore given as:

$$\Phi^{r(i,j)} = r_i + A_i s_i'^P - r_j - A_j s_j'^P = 0 \tag{2.3}$$

Here, A_i is the rotation matrix corresponding to a rotation by an angle ϕ_i about the global frame.

2.3.2 Multibody Method (Iterative Solution)

For the mechanism under consideration,This frame is located at the hip joint as depicted by the revolute joint, D in Figure Figure 2.2 for our model. Notice that the mechanism has six revolute joints, one distance constraint between the hip joint, D and the driver joint, A and one driving constraint as the angular displacement of the driving link. The total number of constraints can therefore be given by $T_c = 2n_r + 2d + d_r$, where n_r is the number of revolute joints, d is the number of distance constraints, and d_r is the number of driving constraints. Here, $n_r = 6$, $d_r = 1$, and $d = 1$, Hence $T_c = 15$. Given estimations of the systems initial configuration,the Newton-Raphson method is used to solve for an initial position that is

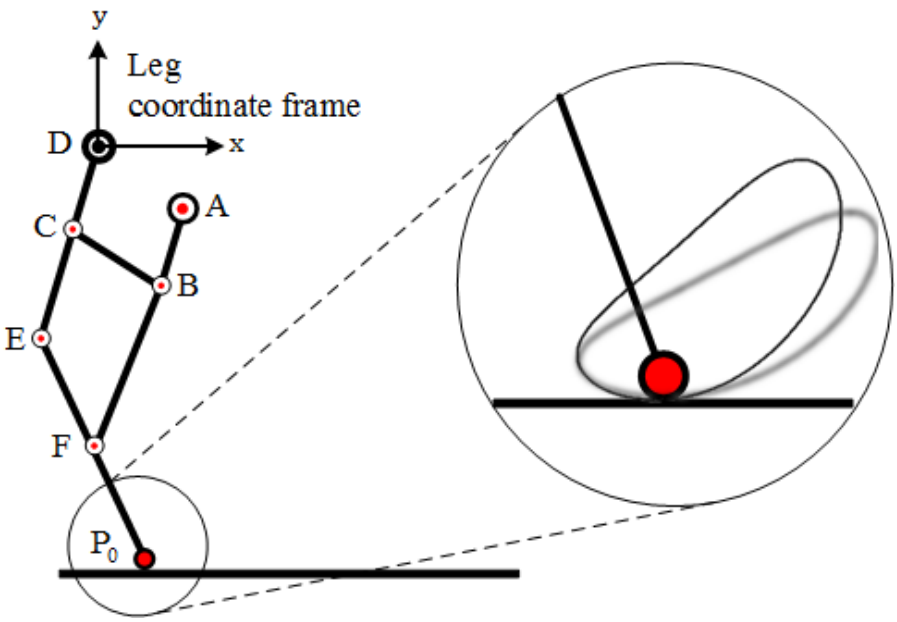

Figure 2.2: Kinematic scheme adopted for the initial design of the mechanism. Shown in the inset are the generated trajectories.

consistent with the constraints specified by Equation 2.3. For the single-DOF mechanism, the crank angle is taken to be the driving input. Based on the value of the driving input, and the initial conditions of the system, the link positions may be computed iteratively as $x_f - x_0 = vt + at^2$ for small time steps, where v and a are given by the velocity and acceleration equations at each time step, given by:

$$\dot{\boldsymbol{q}} = -\boldsymbol{\Phi}_{\boldsymbol{q}}^{-\mathbf{1}}\boldsymbol{\Phi}_{\boldsymbol{t}} \tag{2.4}$$

$$\dot{\boldsymbol{q}} = -\boldsymbol{\Phi}_{\boldsymbol{q}}^{-\mathbf{1}}\gamma \tag{2.5}$$

Where γ is a vector of acceleration independent terms [31]. Here, $\boldsymbol{\Phi}_{\boldsymbol{t}} := \boldsymbol{v}$ and $\boldsymbol{\Phi}_{\boldsymbol{q}}$ is the Jacobian. The generalized positions calculated by the above multibody formulation are used to build a kinematic model to be able to track the foot trajectory of the leg throughout a full step cycle. The dark trajectory in Figure Figure 2.2 depicts the results of the kinematic simulation with heuristically selected link lengths. It can be observed that the trajectory follows a smooth curve. This demonstrates that this mechanism is capable of generating trajectories that minimize ground contact in order to maximize propulsive impulses. However,this trajectory shows that the initially selected parameters (position and orientation) require adjustments to generate a trajectory suitable for trotting.

While the simulated foot trajectory satisfies Requirement 3, further improvement of the link parameters is necessary to arrive at an angle of attack that is more conducive to forward propulsion. In order to reduce the size of the parametric design space, for future optimization, a sensitivity analysis was performed to determine the impact of key parameters on the resultant changes to the angle of attack.

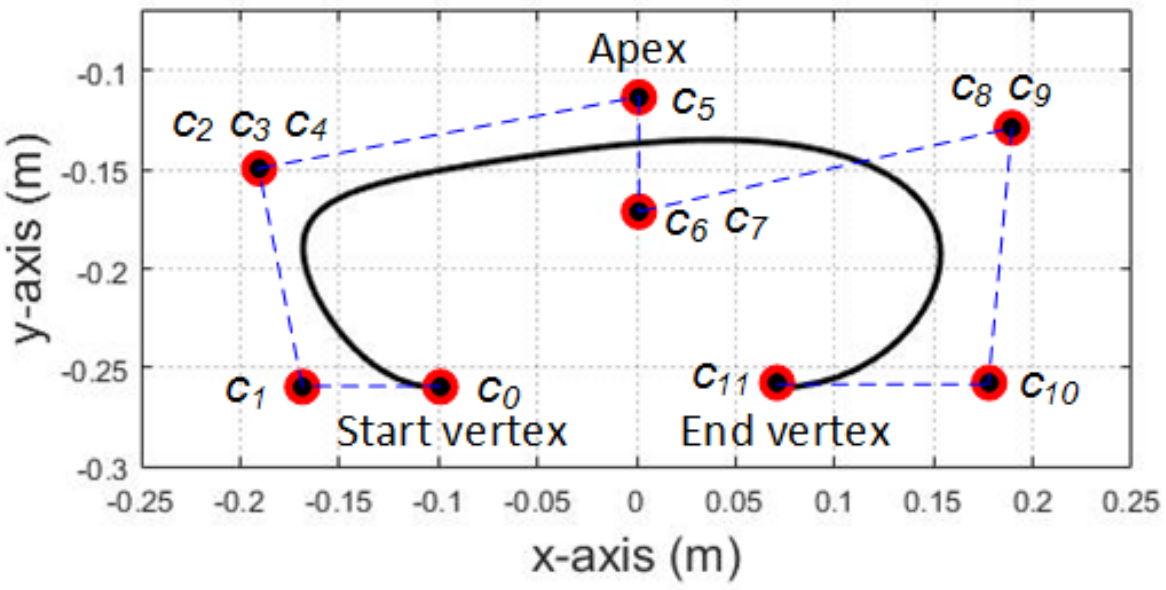

Figure 2.3: Designed trajectory

2.4 Ideal Stride-phase Trajectory Design

The workspace of single DOF legs is constrained by the design parameters (link lengths and configurations); thus, the foot trajectory cannot be altered once the designer determines these parameters. Therefore, optimization is required to trace a favorable trajectory also known as ideal trajectory. In this section, an effort to establish an ideal trajectory is undertaken. For a dynamic gait such as trot, an ideal stance phase curve should be sinusoidal [24] while the swing-phase trajectory is an aspect of careful design. We establish a stance phase trajectory in order to make comparisons with the trajectories generated by the proposed mechanism discussed in Sec. VI. The swing-phase is modeled by a cubic spline using the Bezier curve [32] formulation, expressed as:

$$p_j(t) = \sum_{j=0}^{n} B_j^n(t) c_j \tag{2.6}$$

Table 2.1: Control points utilized in the bezier cure formulation

$Controlpoints$	$x(m)$	$y(m)$
c_0	-0.10	-0.26
c_1	-0.17	-0.26
c_2	-0.19	-0.15
c_3	-0.19	-0.15
c_4	-0.19	-0.15
c_5	-0.19	-0.17
c_6	0	-0.115
c_7	0	-0.115
c_8	0	-0.13
c_9	0.19	-0.13
c_{10}	0.18	-0.26
c_{11}	0.07	-0.26
c_{12}	-0.01	-0.285

For $0 < t < 1$, where $c_j = \{c_0,\ c_1, ..., c_n\}$ is a set of control points defined to produce a specific curve and is the Bernstein basis polynomial of degree n. The control points are initially placed at the beginning, end and apex of the stance phase, and then iteratively weighted to arrive at the desired trajectory. The resulting trajectory should be smooth to avoid perturbations in the system during locomotion. The ideal stance-phase trajectory is as depicted in Figure 2.3.

2.5 Sensitivity Analysis

This section analyzes the effects of varying key link lengths on the foot trajectory, as part of the sensitivity analysis. Further, it establishes metrics to quantify the performance of simulated trajectories with respect to the ideal trajectory established in Sec. III.

To address the challenge of optimizing the vast design space of a six-bar mechanism, prelim-

inary optimization in terms of sensitivity analysis is performed. The result of this analysis is a condensed design space that is conducive to a rigorous optimization process. The kinematic model derived in Sec. IV is modified for the purpose of this analysis to accumulate multiple foot trajectories, their angle of attack, and their stride lengths, creating a library of simulations. Varying position and orientation is a tedious process and one that requires much iteration. Furthermore, the Newton-Raphson method is a time consuming process due to the high-resolution requirements for convergence. We therefore apply the alternative approach of varying the link lengths themselves, thus varying position and orientation of the respective points defining the length. The design space of the lengths is given by the set $\{L_1, L_2, L_3, L_4, L_5, L_6\}$. However, performing a brute-force sensitivity analysis on the complete design space is prohibitively computationally expensive. Instead, we identify two link lengths associated with the crank length, L1 and the distance between the hip joint, located at point A, and the crank joint at point B, L6. As L1 is the driving link and L6 dictates the position of the hip joint relative to the crank joint, these lengths are the most important driving factors of the foot trajectory shape and orientation and as such are the focus of the sensitivity analysis. The parameters for the analyses are varied within a sensible range, which are selected to ensure that the designed leg maintains a compact form factor that satisfies Requirement 5. The heuristically selected link lengths also dictate to what extent the lengths can be varied. Performing simulations beyond these bounds would result in singular configurations and end up adversely affecting the end trajectory to a point where smooth curves are no longer produced. These trajectories are in violation with Requirement 3 and as such are of no interest. The sensitivity analysis is undertaken with a focus on the effects of varying link lengths on angle of attack, 0 and stride length due to their far-reaching effects on stability and distance traversed in one step-cycle.

First, L1 is varied from 0.04 m to 0.08 m; the generated trajectories are stored and overlaid on each other as shown in Figure 2.4 . As shown, the generated trajectory at the upper

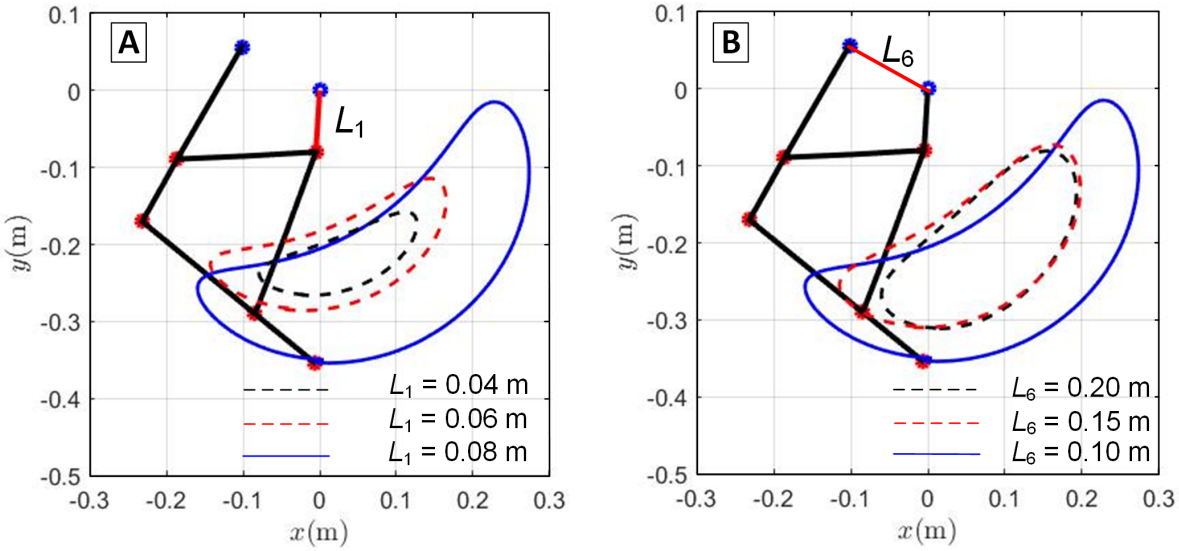

Figure 2.4: Bounded sensitivity analysis: (a) Crank shaft vs Stride length (b) Hip-crank distance vs Angle of attack

limit has a shorter stride length in comparison to that generated by t he lower bound. From the results produce d, a preliminary conclusion is reached that increasing the length L1 increases the stride length. To get a broader perspective of the effect of L1 on the stride length and angle of affect, further simulation studies were conducted and plotted in Figure 2.6. As shown, the preliminary conclusion is proven accurate from the plot. The driver link L1 plotted on the left y-axis has a direct effect on the stride length. It is also evident from the same plot that the angle of attack is minimally affected, resulting in a leg position ahead of the symmetric axis on the hip, thus causing an imbalance during dynamic locomotion. It can be concluded that the longer the radius of the shaft, the longer the stride length. It is to be noted that varying the l ink L1 beyond 0.08m showed irregular trajectories as mentioned earlier. Hence, for this set of heuristic link lengths, L 1 at 0.08m gives a maximum stride length while satisfying Requirements 3 and 5.

The sensitivity analysis on L6 clarifies that varying the value of L6 results in large changes to the orientation of the foot. From the geometry, we can infer that L6 must be greater than L1

or else the links will collide, while Requirement 5 can again bind the upper limits. For these simulations, the upper bound was selected to be 0.20 m and the lower bound to be 0. 10 m, and simulations were performed between intervals of 0.05 m. The results of the simulation are illustrated in **??** and demonstrate that 0 decreases with decrease in the length of L6. Furthermore, too strengthen this observation, a series of simulation studies were performed. The second series of simulations were performed from 0.18 m to 0.06 m at an interval of 0.02 m. The result of this study, as shown in Figure 2.5, reciprocates the results of first set of simulation done on L6. It is worth noting from the same plot, the effect of L6 on stride length is very small. These conclusions were not intuitive and were only established through the application of sensitivity analysis. In conclusion, from these sensitivity analysis studies we learn that the stride length increases with the increase in the length L1 and 0 decreases with the decrease in length L6. It is evident then, that in order to satisfy Requirement 4, the length L6 must be small while remaining larger than L1. There has to be a compromise of stride length to achieve an appropriate angle of attack.

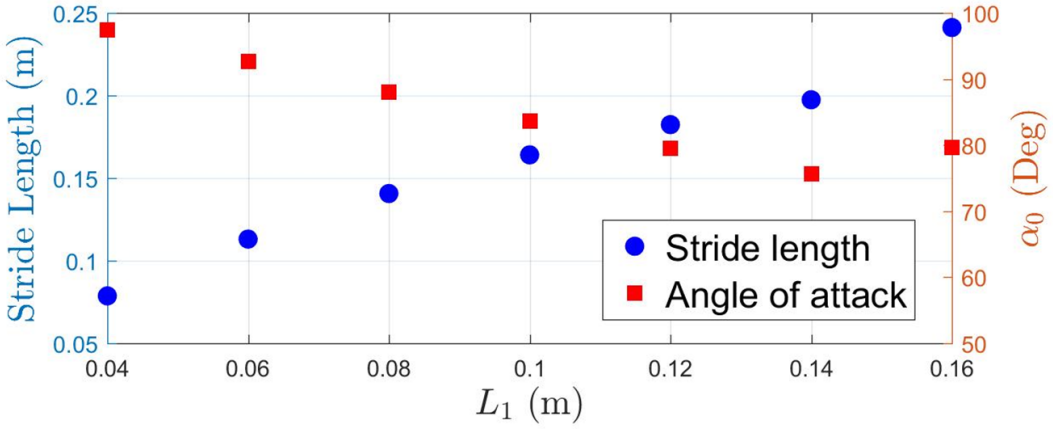

Figure 2.5: Plot showing the effects of varying link lengths L_1

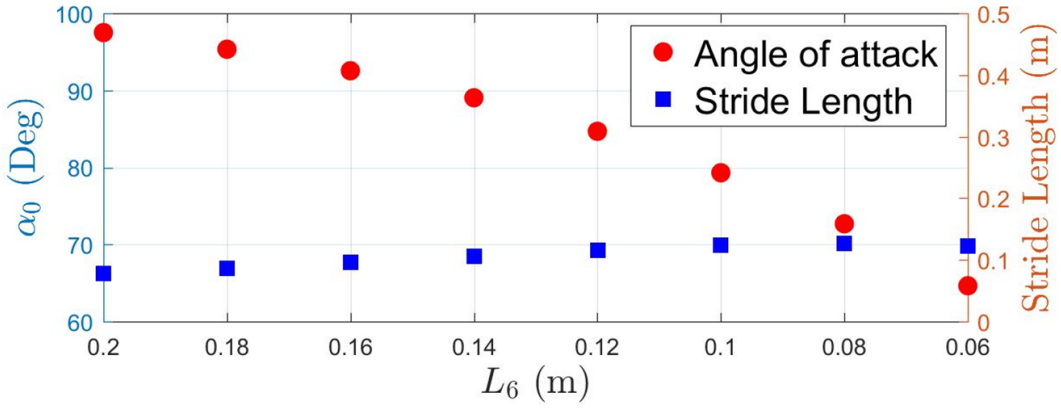

Figure 2.6: Plot showing the effects of varying link lengths L_6

2.6 Comparison Metrics

In order to establish the best trajectory from the library of curves accumulated by sensitivity analysis, a qualitative comparison must be established. It is difficult for a single metric to estimate completely the similarities between two curves. Therefore,in this work, two parameters, the Hausdorff distance [33] and Jaccard distance [34] are employed to quantify the best possible trajectory. The first metric,the Hausdorff distance H(A,B),calculates the Euclidean distance between the two sets of points, in this instance the desired trajectory established in Sec. V, and the trajectory being compared.

$$H(A, B) = max(h(A, B), h(B, A) \tag{2.7}$$

In, Equation 2.7 $h(A, B)$ is the directed Hausdorff distance from set A to set B. From the generated library, smooth trajectories were selected, the Hausdorff distance was then computed, and the results are recorded in Table 2.2. As shown, the distance between the ideal and comparable trajectory is at a minimum for $L_1 = 0.04m$ and $L_6 = 0.06m$, indicating that this particular curve among all the curves is closest to the ideal. However, this index

Table 2.2: Hausdorff distances of the simulated trajectories

L_1	L_6	$H(A,B)$	L_1	L_6	$H(A,B)$
0.04	0.2	0.19	0.04	0.14	0.15
0.06	0.2	0.16	0.04	0.12	0.13
0.08	0.2	0.13	0.04	0.1	0.1
0.1	0.2	0.11	**0.04**	**0.06**	**0.084**

* All units are in meters

does not consider the length or orientation of the curve; therefore we cannot discern from this metric any information on whether the indicated ideal is encompassing, encircled by, or tangent to the desired curve. Another metric is therefore introduced to further quantize the generated trajectories. This metric compares the similarity of the two sets, A and B and is known as Jaccard similarity index. It calculates the Jaccard distance J_d, which is a measure of the dis-similarity between the sets.

$$J_i = \frac{A \cap B}{A \cup B} \tag{2.8}$$

Table 2.3: Jaccard distances of the simulated trajectories.

L_1	L_6	d_j	L_1	L_6	d_j
0.04	0.2	0.1446	0.04	0.14	0.1352
0.06	0.2	0.1486	0.04	0.12	0.1278
0.08	0.2	0.1566	0.04	0.1	0.1234
0.1	0.2	0.1665	**0.04**	**0.06**	**0.1148**

* All units are in meters

This can be established by first calculating the Jaccard index J_i, defined as in Equation 2.8. Further, $J_d = 1 - J_i$. The Jaccard distances are calculated for the same simulated trajectories as above and are shown in Table 2.3. The minimum value for $J_d, 0.1148$, corresponds to L_1

of 0.04 m and L_6 equal to 0.06 m. This indicates that curves generated by these parameters most closely resemble the ideal trajectory. This finding corroborates with the result obtained from Table 2.2. This trajectory, pictured in Figure 2.7, is closest to the ideal of those contained within the curves generated by the selective optimization of link lengths L_1 and L_6. The angle of attack in this configuration, $\alpha_0 = 64.64°$, is in the range of stable running established in [30]. This result will be used as a starting point for parametric optimization in chapter 3 to determine the remaining optimum design parameters.

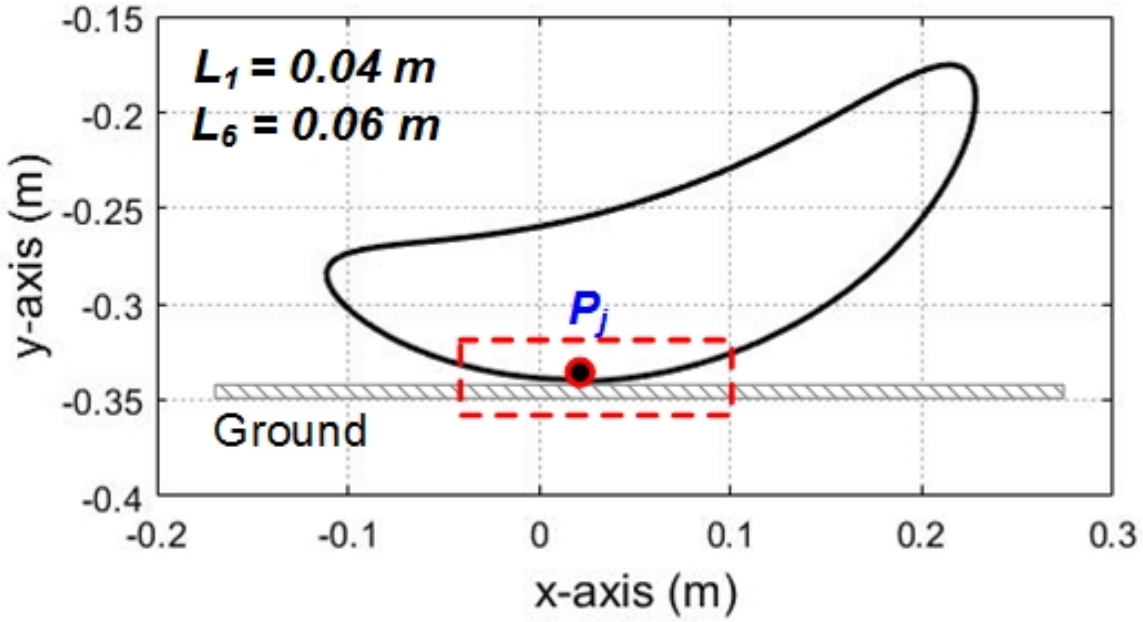

Figure 2.7: Realization of the best trajectory from the simulated trajectories.

2.7 Discussion

This chapter presented a novel, single DOF leg mechanism in an effort to realize a dynamic gait while reducing mechanical and control complexity. A study is then conducted to identify

crucial parameters of the design that affect the foot trajectory. Results of sensitivity analysis indicate that: (1) variations of crank radius proportionally affect the stride length, and (2) the variation of the distance between the hip and crank joint inversely affects the angle of attack. Moreover, with help of curve metrics, the trajectory closest to the designed ideal trajectory is identified. Future work will include optimization of the dimensional parameters identified in section 2.6 to synthesize a gait that more closely generates the idealized swing-phase path. A leg prototype will be developed and its performance tested. Moreover, a quadruped integrating the proposed leg will serve as an experimental platform to study the performance enhancements that robotic tails provide.

Chapter 3

Design and Optimization

While the analysis in chapter 2 has provided us with insightful information, the trajectory is still not satisfactory enough. Towards meeting requirement 5 in totality, we perform a complete parametric optimization on the design space of the mechanism. The optimization and the corresponding results are detailed in this chapter.

3.1 Design Evolution

The mechanism presented in chapter 2 has a set of 9 design parameters composed of 8 link lengths and one angle that have to identified before a prototype can be made. This chapter provides an explanation for the optimization process we undertook to obtain a mechanism that meets completely the requirements established in the previous section. based on the observations and lessons learned from the previous section, it is clear that a minimal angle of attack is preferable for forward locomotion. According to Geyer's [30] observation an angle between 50° to 70°. Furthermore, a larger stride length is desired.

3.1.1 Objective function

This section establishes the objective function and shows the optimized design variables as results $P = [a, b, c, d, e, f, g, h, l_t]$. Based on our requirements established a multi-objective cost function: The first objective penalizes any design that has a angle of attack steeper than 64°. The second objective function rewards a smooth, closed loop curve from the start to the end of the cycle. The objective function can then be formulated as

$$Y(P) = W_1 * \frac{1}{min(\alpha_0)} + W_2 * \sum_{\theta_4=0}^{360} (p - p_{des})^2 \tag{3.1}$$

p_{des} is acquired from the ideal trajectory mentioned in earlier chapter. However, at the same time the trajectory should also maintain a minimal angle of attack, the inclusion of $alpha_0$ into the objective function is to precisely do the same. her min(α_0) is the minimum value of the variable α_0 over the entire cycle. the function p_des assumes the same quadratic description in chapter 2.

Further equality constraints are specified in the model to obtain a closed loop solution with realistic design variables. We introduce a function $Y(P) = K$ the set of parameters P for a geometric solution that is non-existent. Further based on the sensitivity analysis, inequality constraints are specified for the link lengths l_1 and l_6.

$$\begin{aligned} 0.04 \leq l_1 \leq 0.1 \\ 0.04 \leq l_6 \leq 0.1 \end{aligned} \tag{3.2}$$

The main goal of this parameteric optimization is to get a trajectory that has minimal angle of attack, the values of the obtained design variable is detailed in Table 3.1. Further to validate the results an obtain a kinematic mapping vector loop analysis is performed.

Table 3.1: Optimized Design Variables

links	*Heuristic*	*Optimized*
a	164	80
b	95	80
c	180	105
d	40	20
e	180	53
f	85	130
g	62	50
h	230	190
l_f	180	210
l_t	290	303

* All units are in mm

3.2 Kinematic mapping

Traditional multi-DOF leg controllers have the burden of realtime inverse kinematic (IK) calculations to estimate the motion each joint has to undertake in order to perform a single step, this is on top of the higher-level dynamic controllers the system has to run in order to be able to balance, perform path planning itself. Although, it is not possible to avoid the underlying dynamic calculations to build reliable controllers, BOLT mechanism allows the simplification of the kinematic calculations, thus partly reducing the computational burden. Owing to the mechanical constraints and the simplicity of a continuously rotating link, the IK problem of this mechanism is simply a one to one mapping between the driving link and the end-effector. To elaborate for any angle the driver makes with respect to the $x - axis$, there is a unique position in the $x - y$ plane the end effector assumes. Thus in terms of implementation and computational burden this is a very big advantage. Note that the method used in subsection 2.3.2 is an iterative method and results in a open loop trajectory. To avoid this drift, a careful selection of the solver tolerance has to performed. Usually,

this is a heuristic and their is no scientific method one could resort to make such selections. Therefore we stray from this method in lieu of achieving a closed loop trajectory, we look to the alternative of vector-loop analysis. This section apart from establishing the one-to-one mapping also validates the optimization results undertaken in section 3.1 .

3.2.1 Vector loop method

The vector loop method is a commonly used method for the kinematic analysis of planar mechanisms that are too cumbersome to describe by simple trigonometric equations, however one disadvantage is that the extension of this model for dynamic calculations are not that fruitful. Since we have already established a multibody model in the earlier section and the purpose of this section is to just arrive at the kinematic mapping, we resort to vector loop analysis. To begin, the model assumes the same terminology as used in subsection 2.3.2. As evident from Figure 3.1, the mechanism is made up of two vector loops. First, let us consider the loop formed by the the links AC, CE, BE and AB. These are represented by vectors $\vec{R_1}$, $\vec{R_2}$, $\vec{R_3}$ and $\vec{R_4}$ respectively. The equation thus representing this loop can be described by Equation 3.3

$$\vec{R_1} + \vec{R_2} + \vec{R_3} + \vec{R_4} = 0 \tag{3.3}$$

Note that, the lengths of the links comprising loop 1 are all known to us. Further the angle link AC makes with respect to the horizontal is fixed. Along with that the driving angle is manipulated from 0° to 360° is of knowledge the model. Therefore, the problem boils down to finding the two unknown angles θ_2 and θ_3 with two equations that can be written by

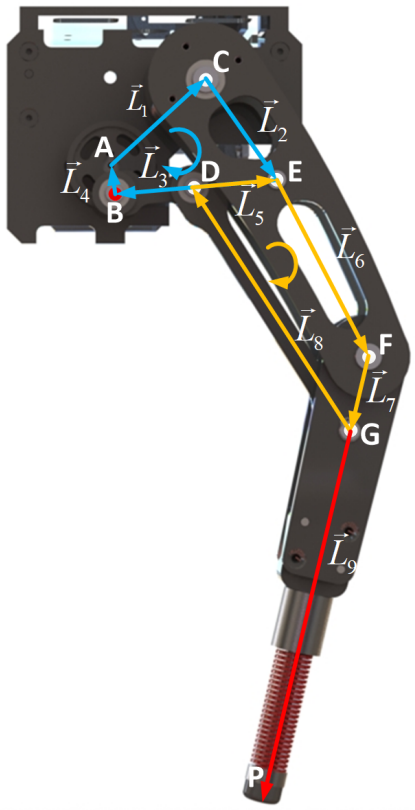

Figure 3.1: Kinematic model used for the vector-loop analysis

decomposing the real and imaginary parts of euler formula as in Equation 3.4

$$\begin{aligned} acos(\theta_1) + acos(\theta_2) + acos(\theta_3) + acos(\theta_4) = 0 \\ asin(\theta_1) + asin(\theta_2) + asin(\theta_3) + asin(\theta_4) = 0 \end{aligned} \tag{3.4}$$

These two non-linear algebraic equations(AE) can then be solved for the two unknowns using the "fsolve" function in MATLAB. For the sake of completeness the closed form solution of

θ_2 can be written down as:

$$\theta_{2_{1,2}} = 2\arctan\{\frac{-2R \pm \sqrt{4R^2 - 4(W+Q)(W-Q)}}{2(W-Q)}\}$$
$$R = -\left|\vec{R_3}\right|^2 + \left|\vec{R_1}\right|^2 + \left|\vec{R_2}\right|^2 + \left|\vec{R_4}\right|^2 + 2\left|\vec{R_1}\right|\left|\vec{R_4}\right| cos(\theta_1)cos(\theta_4) + 2\left|\vec{R_1}\right|\left|\vec{R_4}\right| sin(\theta_1)sin(\theta_4)$$
$$W = 2\left|\vec{R_1}\right|\left|\vec{R_2}\right| cos(\theta_1) + 2\left|\vec{R_2}\right|\left|\vec{R_4}\right| cos\theta_4$$
$$Q = 2\left|\vec{R_1}\right|\left|\vec{R_2}\right| sin(\theta_1) + 2\left|\vec{R_2}\right|\left|\vec{R_4}\right| sin\theta_4 \tag{3.5}$$

In the same manner one can computer for θ_3 as in Equation 3.6

$$\theta_{3_{1,2}} = 2\arctan\{\frac{-2U \pm \sqrt{4U^2 - 4(M+N)(M-N)}}{2(M-N)}\}$$
$$U = -\left|\vec{R_2}\right|^2 + \left|\vec{R_1}\right|^2 + \left|\vec{R_3}\right|^2 + \left|\vec{R_4}\right|^2 + 2\left|\vec{R_1}\right|\left|\vec{R_4}\right| cos(\theta_1)cos(\theta_4) + 2\left|\vec{R_1}\right|\left|\vec{R_4}\right| sin(\theta_1)sin(\theta_4)$$
$$W = 2\left|\vec{R_1}\right|\left|\vec{R_3}\right| cos(\theta_1) + 2\left|\vec{R_3}\right|\left|\vec{R_4}\right| cos\theta_4$$
$$Q = 2\left|\vec{R_1}\right|\left|\vec{R_3}\right| sin(\theta_1) + 2\left|\vec{R_3}\right|\left|\vec{R_4}\right| sin\theta_4 \tag{3.6}$$

In the end two solutions are obtained for both θ_2 and θ_3. Based on the notation and the quadrant the system is defined in, the correct solution is obvious. If the formulation is done with care, the fsolve outputs the correct solution right off the bat. We can then solve loop 2 comprising of links DE, EF, FG and GD. On inspection it is evident that $\theta_5 = \theta_3$ and $\theta_6 = \theta_2$. As a result of the parametric optimization we have the all the link lengths required. We can then isolate this loop and utilize the same formulation as above and solve for θ_7, representing the angle of the knee with respect to the horizontal and θ_8, representing the KFE angle. With valid justification, it can then be said that the mechanical constraints of loop 1 is encoded in θ_2 and the constraints applied on the knee are captured by θ_7. At this point, the mechanism is kinematically equivalent to the classic two link manipulator as illustrated in Figure 3.2. The end effector trajectory can then be effectively computed by

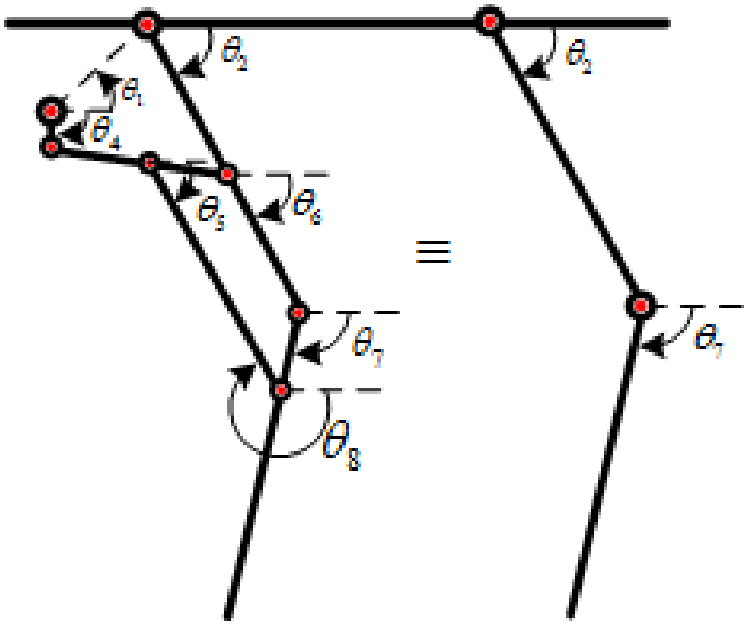

Figure 3.2: Illustration of kinematic equivalence after performing vector loop analysis

the common equation Equation 3.7.

$$\begin{aligned} l_2 * cos(\theta_2) + l_7 * cos(\theta_7) = 0 \\ l_2 * sin(\theta_2) + l_7 * sin(\theta_7) = 0 \end{aligned} \tag{3.7}$$

We have now arrived at the forward kinematics (FK) solution for the BOLT mechanism. Since, the mechanism is capable of executing only one trajectory, a look up table like implementation is justified. The look up table can then be used in both FK and IK implementation. By following, this approach the need for online solving of algebraic equations during real-time implementation is eliminated and the IK problem is substantially simplified.

3.2.2 Results

Kinematic simulation implementing the vector loop analysis result in a closed loop trajectory that very closely matches the established reference trajectory in section 2.4, as results in **??**

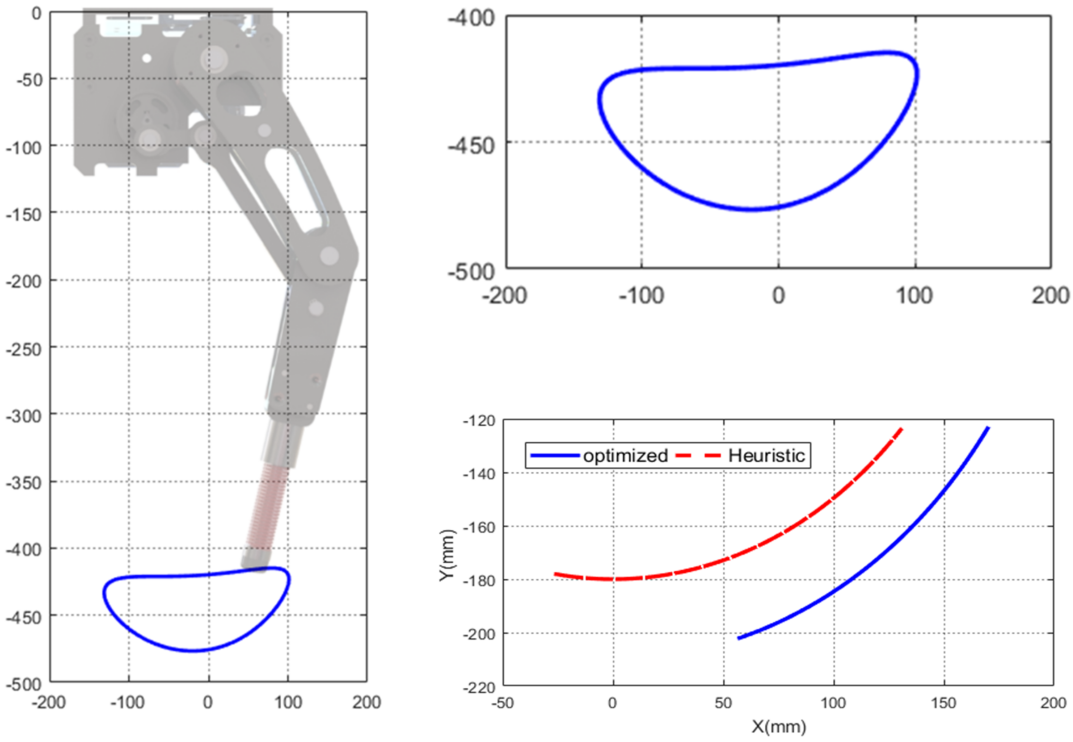

Figure 3.3: a)illustrating the optimized leg executing the optimized trajectory. (b) Trajectory executed by the mechanism prior and after optimization (c) Close up view of the optimized trajectory

indicate. On inspection of Figure 3.3(b), the success of the undertaken optimization process is evident. The trajectory traced by the mechanism as a result of heuristic link lengths is in red and runs into the negative axis. From the adapted co-ordinate frame, this violation is clear evidence of steep angle of attack resulting in tripping and falling over. However, the blue trajectory executed by BOLT's Knee is restrained to the positive quadrant is an indication of the fast-running capacity the mechanism holds. Further, evidence is provided in Figure 3.5. The angular displacement of the hip, knee and HFE and KFE joints

are superimposed with the angular profile followed by the joints of the mechanism designed with the heuristic link lengths. Key observation to be taken into account is the minimal jump in angular displacements of the optimized mechanism indicating less energy expenditure.

This is elucidated in Figure 3.5 (a) and Figure 3.5 (c) that correspond to the hip and knee angular profile. The profile of the HFE and KFE link stay the same with an offset.

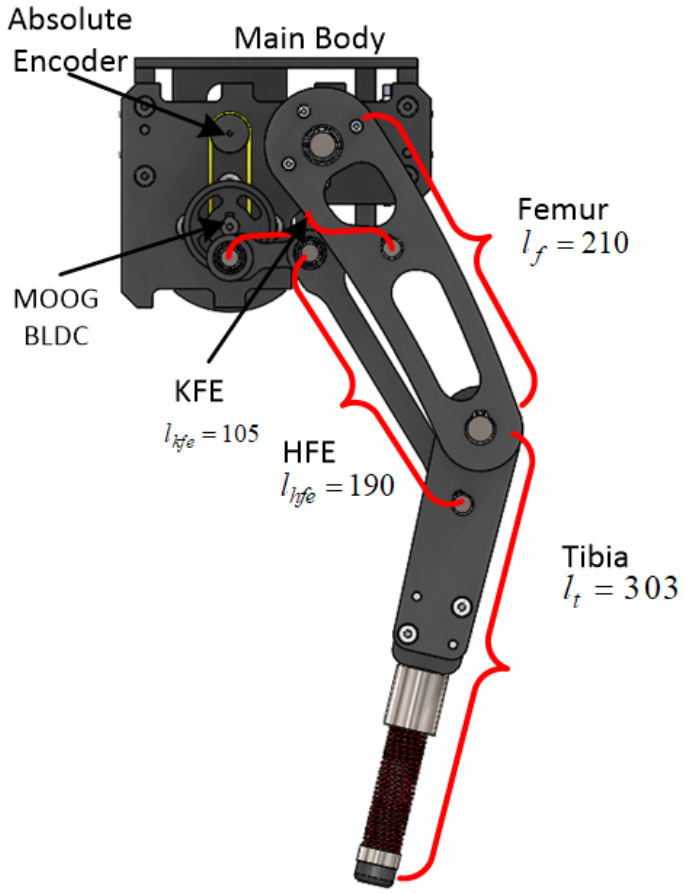

Figure 3.4: 3D rendering of the optimized Leg (BOLT)

3.3 Robotic leg Design

The single leg is depicted in Figure 3.4.Based on the lessons, learned from the literature and the primary design goals established in chapter 2, the emphasis was to lightweight construction utilizing aerospace grade Al 6061. In addition, this ensures the inertia of the moving segments are minimal.The motor is placed close to the hip and the motion is transmitted to

the hip and knee with the lightweight HFE and KFE links. The designed system features a very high -power to weight ratio, with the entire system weighing around 4kg. The mobility of the hip flexion, extension angle is from$[-70^{\circ}, + +70^{\circ}]$.

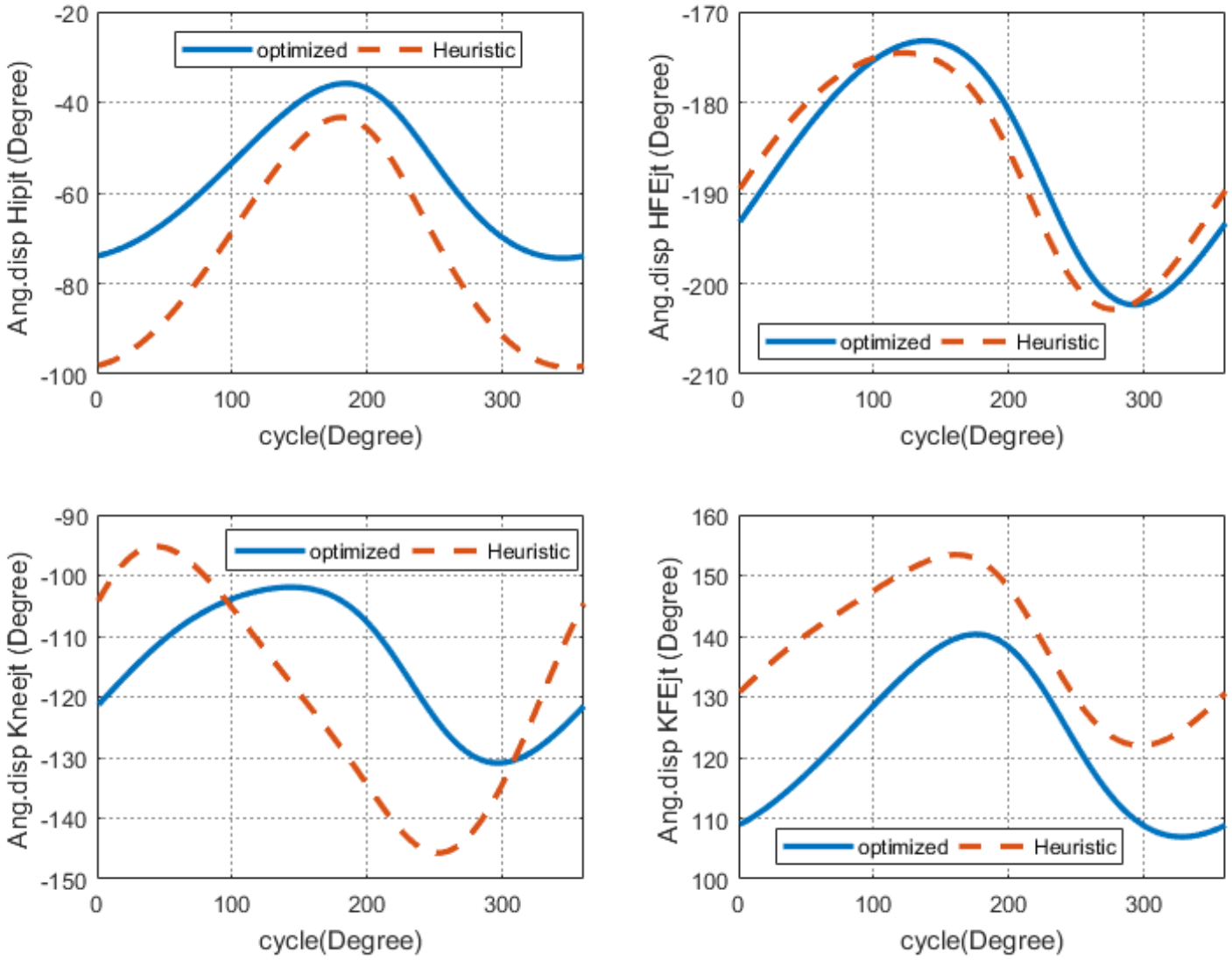

Figure 3.5: Angular displacements before and after optimization

Chapter 4

Single Leg Dynamics of BOLT

Now, with a clear understanding of the leg's motion in space with the help of kinematics, as described in chapter 3. In this chapter, we strive to realize the dynamic model that maps the forces and torques of this floating base robot, i.e a robot that is free to move in space by manipulating the ground reaction forces unlike traditional industrial manipulators.
Here, we resort to the Lagrangian formalization to establish the mathematical description, which is repeated here for convenience. The Lagrangian, L is summed up in Equation 4.1.

$$L = T - V \tag{4.1}$$

Here, T denotes the total kinetic energy of the system and Vrepresents the total potential energy of the system. Further to obtain equation of motions (EOM), adopt Equation 4.2

$$\frac{d}{dt}\left(\frac{\partial L}{\partial \dot{q}_i}\right) - \frac{\partial L}{\partial q_i} = 0 \tag{4.2}$$

However, it is shown in this chapter that Equation 4.2 is alone not sufficient to give a complete description of the system, owing to the closed loops present in the mechanism and further

describes existing methods that address the modeling of closed kinematic chains (CKC). These methods have limitations that impede model-based controller designs. Therefore this chapter, establishes an extension of a new method, Singularly perturbed formulation (SPF) that surpasses all the limitations experienced during modeling CKC.

4.1 Mathematical description

Following the Lagrangian method described above, the general dynamic EOMs of a floating base system with n links in independent generalized coordinates, denoted by the vector $q \in R^{n_q}$, canonically are written down as:

$$H(q)\ddot{q} + C(q,\dot{q})\dot{q} + G(q) = B\tau + J_c(q)^T F_{ext} \tag{4.3}$$

where $H(q) \in R^{n_q \times n_q}$ represents the generalized mass matrix, $C(q,\dot{q}) \in R^(n_q)$ contains the Coriolis and centrifugal terms,$G(q) \in R^{n_q}$ is the gravitational term, B is the input matrix, $\tau \in R^{n_q}$ is the torque vector provided by the actuators and $J_c(q)^T$ is the jacobian that maps the extenal forces, F_{ext} to the generalized co-ordinates. Finally, Equation 4.3 results in second-order ordinary differential equations (ODEs) identical in dimension to the number of degrees of freedom of the system. This implies that for each DOF there is an independent control input. Furthermore, this formulation possesses several structural properties that are favorable in control design [35]. It is therefore favorable, if possible to describe the EOMs of a system in this form.

However, CKCs like BOLT are characterized by algebraic equations (AE) and the resultant systems of equations that describe the system are identified as differential algebraic equations (DAEs). From the simulation standpoint, numerical solutions of DAEs are hard to obtain in comparison to ordinary differential equations (ODEs) [36]. Within robotics, the constrained

mechanisms are defined by index-3 DAEs [37]. By definition, index represents the number of times holonomic constraints have to be differentiated with respect to time before the form of ODE can be assumed. One of the existing methods in literature proposes direct interaction with index-3 DAEs through input-output linearization [38]. Other technique, suggests differentiation of holonomic constraints twice, thus representing them at the velocity level and then solving the AE to obtain an implicit state space representation of the resultant index-1 DAE [39]. However, a by-product of this method is the magnification of the drift in solution and furthermore, the admissibility of the result is solely dependent on the satisfaction of the initial condition. Drift stabilization formulations have been proposed in the past [40], [41] to address this issue. Amongst these, Baumgartes stabilization method is a widely adopted scheme. Yet, its appeal is shadowed by the difficulty of choosing appropriate parameters that guarantee robustness [42]. Moreover, from the control perspective, as noted in [43], a rich library of stable model-based controllers exist for dynamics represented by ODEs in explicit state space form but are not readily extended to DAE descriptions that are implicit in nature. This is a vast topic that escapes the scope of this thesis; therefore for an in-depth analysis, interested readers are pointed to [44], [45].

Hence, towards the effort of approximating the DAE EOMs of BOLT as ODEs with the aim of surpassing all the above elucidated limitations, we introduce an extension of SPF to floating base systems. The preceding sub-sections describes the systematic approach undertaken to approximate the DAEs of the CKC leg mechanism as ODEs in independent coordinates. Figure 4.1 elucidates the purpose of this section.

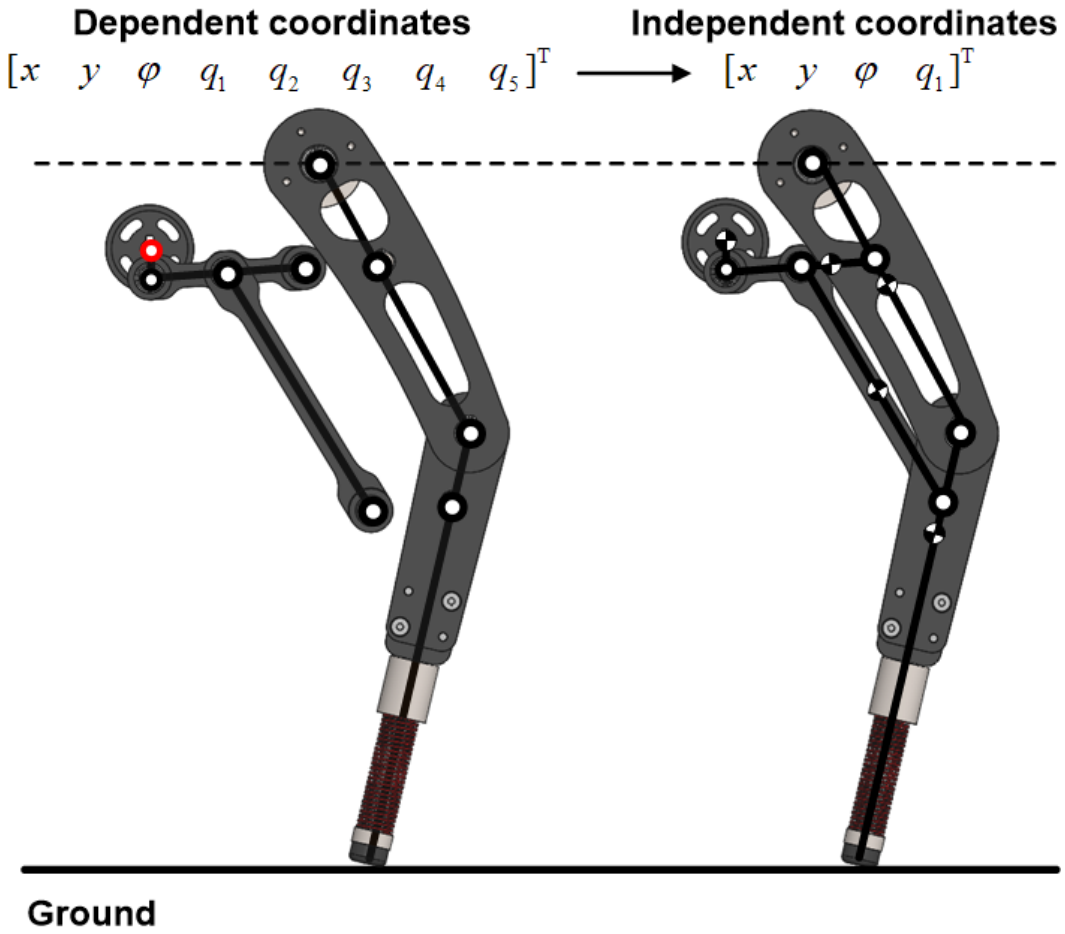

Figure 4.1: Illustrating the virtual separation method adopted to alleviate modeling of CKC mechanism on the left. Towards the right the rejoining is performed once the reduced order state space model is achieved.

4.1.1 Underlying Equations of Motion

The method of virtual separation, as in [46], is adapted to derive the dynamic model of the CKC mechanism under consideration. First, this method prescribes separation of joints at strategic locations to form serial and branched kinematic chains as highlighted in Fig. 1. In this work, such a system is denoted as an unconstrained system. Traditional methods used for serial chains can then be adopted to formulate the unconstrained systems EOMs. To capture the dynamic configuration of this floating base system, two coordinate frames are

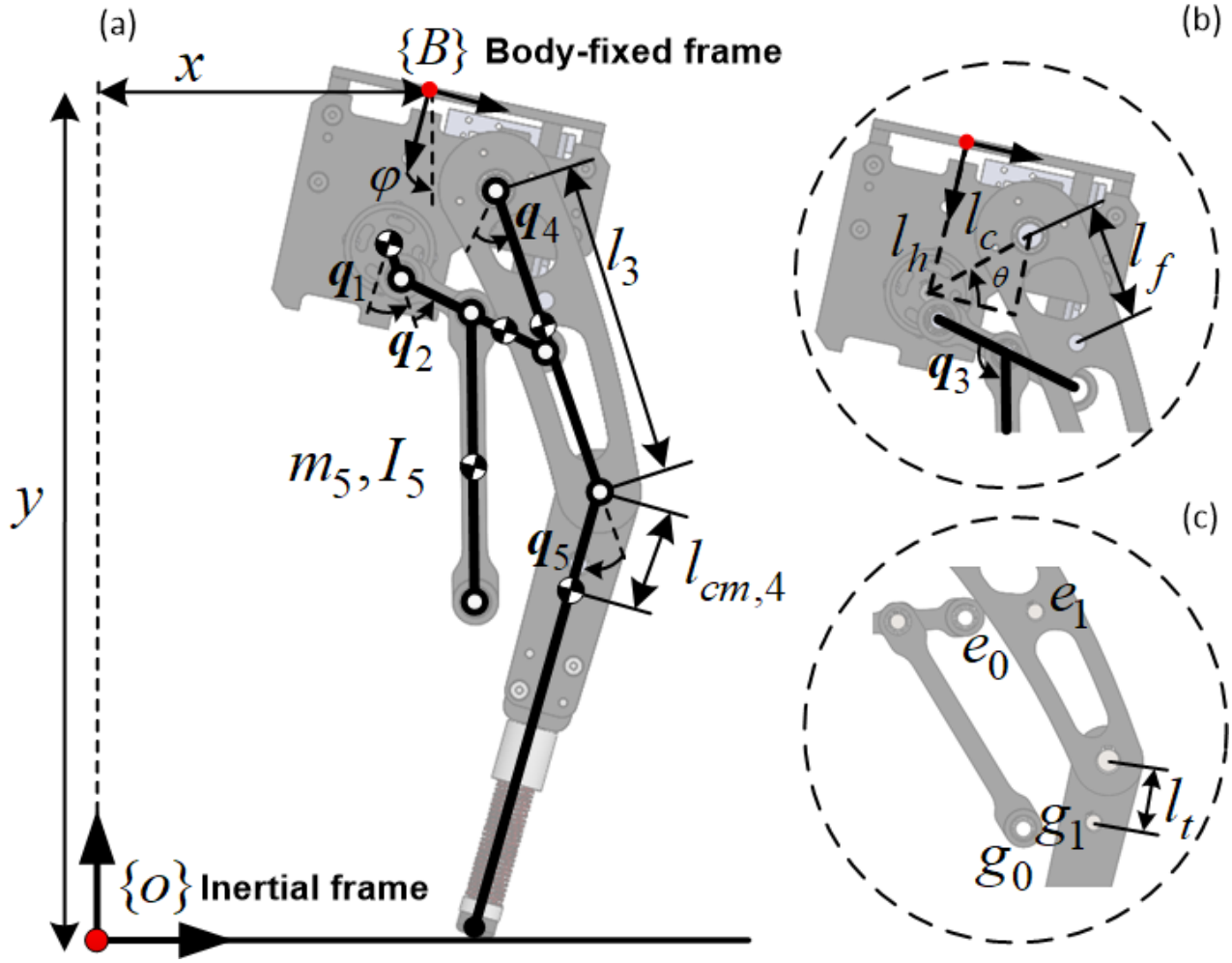

Figure 4.2: Schematic model of BOLT denoting the nomenclature used to derive the dynamic description.

defined, an inertial reference frame O and a body fixed frame B. The global position of the frame B is given by x and y and encodes the orientation of the frontal plane with respect to frame O. Each links configuration relative to its previous frame is represented by q_i with $i = 1, , 5$. These variables are collected to form a vector of dependent coordinates $q_d := [x\ y\ \phi\ q_1\ q_2\ q_3\ q_4\ q_5]^{T^{-1}}$ and are illustrated in Figure 4.2. With the help of a Lagrangian formulation, the EOMs of the unconstrained system in dependent coordinates are then given by Equation 4.4

$$H'(q_d)\ddot{q_d} + C'(q_d, \dot{q_d})\dot{q_d} + G'(q_d) = B\tau + J_c'(q_d)^T F_{ext} \tag{4.4}$$

Here, $H(q) \in R^{8\times8}$, $C(q, \dot{q}) \in R^8$ and $G(q) \in R^8$ are, respectively, the mass, Coriolis, and gravitational matrices in the model of the unconstrained system. Next, separated joints must be reconnected. This method dictates the incorporation of constraint equations given by $\phi(q_d)$ into the mathematical description of the system. Constraint definitions are given in Figure 4.2 c. The result is a DAE that completely characterizes BOLT and takes the form of Equation 4.5.

$$\begin{aligned} H'(q_d)\ddot{q_d} + C'(q_d, \dot{q_d})\dot{q_d} + G'(q_d) &= B\tau + J_c'(q_d)^T F_{ext} \\ \phi(q_d) &= 0 \end{aligned} \tag{4.5}$$

4.1.2 Singularly Perturbed Formulation (SPF)

Due to the kinematic coupling present in the mechanism, q_1 alone is sufficient to describe the legs motion. Thus, q_1, along with the global position and orientation of the robot, are the only generalized coordinates necessary to describe the system, and are collected in the vector, $q := [x\ y\ \varphi\ q_1]^T$. From here forth, the dependent variables are represented by $Z := [q_2\ q_3\ q_4\ q_5]^T$. To eliminate the first order derivative terms of z from Equation 4.5 and obtain an explicit description of the CKC robot, the singularly perturbed dynamic model for fixed base models as in [47] is adapted to this floating base dynamic model.

To begin, we will consider two selector matrices S_q and S_z to encapsulate the relationship that q and z hold with q_d. This correlation can be denoted as, $[q\ z]^T = [S_q\ S_z]^T q_d d$. From this point on, q_d is replaced by q_z . Given that this minimal order model revolves around the representation of DAEs as ODEs, the problem hinges upon the approximation of the algebraic constraints. Drawing from the work in [5], we therefore introduce a variable

$\dot{w} := \phi(q,\ z)$ to capture the degree of constraint violation. Ideally, it is desired for this value to asymptotically converge to 0. By nature, w is an arbitrary variable, allowing the flexibility to decide its dynamic behavior. Hence, we designate $\dot{w} = -1/\varepsilon w$ to assure convergence to the invariant set $\{0\}$. Here,ε can accommodate any small positive number. By definition of w, this relationship can then be rewritten as

$$J_z\dot{z} + J_q\dot{q} = \frac{1}{\varepsilon}\phi(q,\ z) \tag{4.6}$$

where J_z and J_q are the Jacobian matrices. Note that the inclusion of Equation 4.6 introduces fast dynamics into the model, thus eliminating the algebraic equations.

However, the governing ODE in Equation 4.5 is still coupled with the second order terms of the dependent variables in z. Therefore, a dimensionality reduction process is undertaken. First, two terms Φ and P are introduced.

$$\Phi(q,\ z) := \begin{bmatrix} \phi(q,\ z) \\ S_q(q,\ z) \end{bmatrix} \tag{4.7}$$

$$\rho(q,\ z) = \dot{\Phi}^{-1}(q,\ z) \begin{bmatrix} 0 \\ I_{n_q \times n_q} \end{bmatrix} \tag{4.8}$$

We can then define $(\dot{q}, \dot{z}) = \rho(q,\ z)\dot{q}$, the proof of which is divulged in [45]. With this in mind, the deformation can then be performed by noting Equation 4.10. Here, for the sake of brevity, external forces are omitted. This can be verified by observing the real coordinate spaces: $H(q) \in R^{4\times4}$, $C(q, \dot{q}) \in R^4$ and $G(q) \in R^8$. Finally, the model can be pieced together by combining Equation 4.6 and Equation 4.10, and the external force terms, and is denoted as:

$$J_z(q,\ z)\dot{z} = \frac{-1}{\varepsilon}\phi(q,\ z) - J_q(q,\ z)\dot{q} \tag{4.9}$$

Equation 4.9 is the ODE approximation of the BOLTs dynamic model.

$$\begin{aligned} H(q,\ z) &= \rho(q,\ z)^T H'(q,\ z)\rho(q,\ z) \\ C(q,\dot{q},z,\dot{z}) &= \rho(q,\ z)^T C'(q,\dot{q},z,\dot{z})\rho(q,\ z) + \rho(q,\ z)^T H'(q,\ z)\dot{\rho}(q,\dot{q},z,\dot{z}) \\ G(q,\ z) &= \rho(q,\ z)^T G'(q,\ z) \end{aligned} \tag{4.10}$$

We now arrive at more manageable equations to describe the motion of the BOLT mechanism. Further treatment is shown to arrive at the stance phase and flight phase dynamic equations as described in the appendix.

Chapter 5

Experimental validation

5.1 Experimental Setup

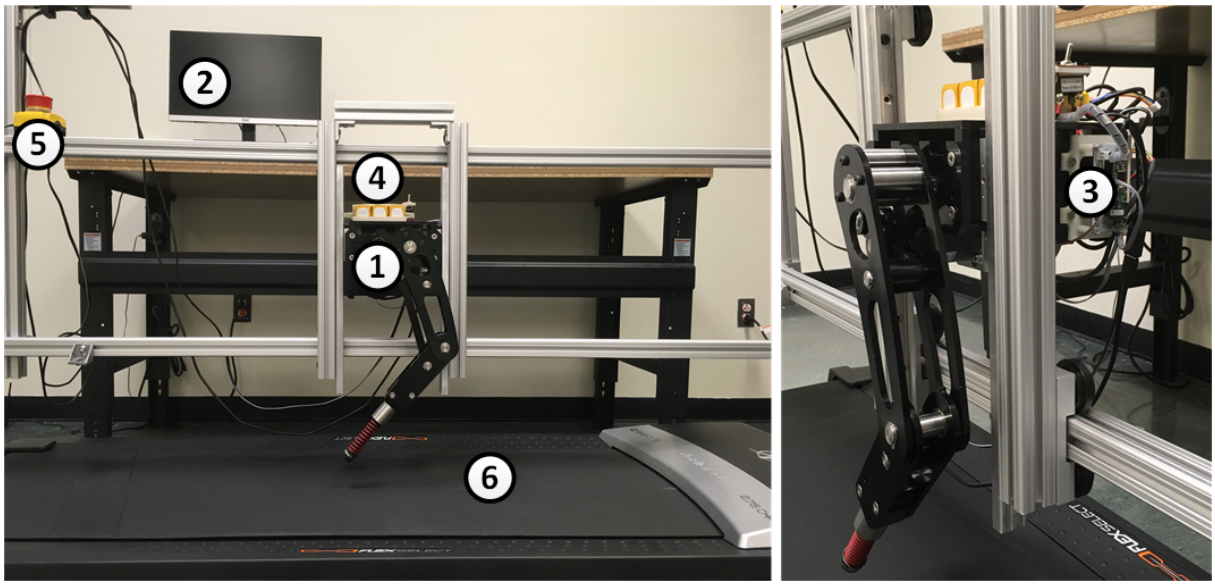

Figure 5.1: Setup for testing BOLTs running gait: 1) BOLT, 2) Higher level controller, 3) Low-level controller, 4) LiPo batteries in series, 5) Emergency stop, 6) Treadmill.

The robot is constrained to the sagittal plane and is allowed motion only in $x-y$ direction as

shown in Fig. 6. It is actuated by a BLDC motor that is mounted with a 2 stage 32:1 gear reduction, planetary gearbox. Three 14.8 V LiPo batteries are connected in series (32.56 Whrs) to power the robot. It harbors a 10-bit absolute encoder to receive the positional feedback data of the crank shaft. The one-to -one mapping established in chapter 3 can now be utilized with the help of encoder feedback. The setup is mounted onto a commercially available treadmill to perform a series of experiments and to test controller performance. For now, the setup will evaluate the capabilities of BOLt's running performance in open loop. The system architecture boasts a micro-controller, teensy to perform low-level calculations. The setup allows the higher-level controller running on a remote PC to transmit low-level commands to the Teensy micro controller.This architecture will be modified in the process of preparing the system for out of the laboratory test setting.

5.2 Trajectory Validation experiment

To validate the results of the topological optimization presented in **??**, a trajectory tracking experiment is performed. For this, experiment, we used a custom made object tracking system, Linear Optical sensor array in our lab owing to its mm level accuracy [48]. The tracker's optimal functioning range is at a distance of 2800mm from the object. The marker, the electronics unit that transmits data to a remote PC were then all mounted securely onto the system. The marker was placed at the foot and battery and electronics unit away from the foot. To avoid damage to the sensor, BOLT was suspended in air thus avoiding any sort of ground contact. The robot was then first run at slow speeds and the corresponding in Figure 5.2 a is plotted. As is evident from the graph that the trajectory has symmetrical stance phase trajectory. Further, the leg was run at its maximum speed of 3.2 m/s. The tracker was able to capture the resultant trajectory as shown in Figure 5.2 b. However, due

to the international rotation of the tracker, there are visible errors in the trajectory. On close observation this experiment also reveals the stride length to be 220mm and stride height to be 50mm.

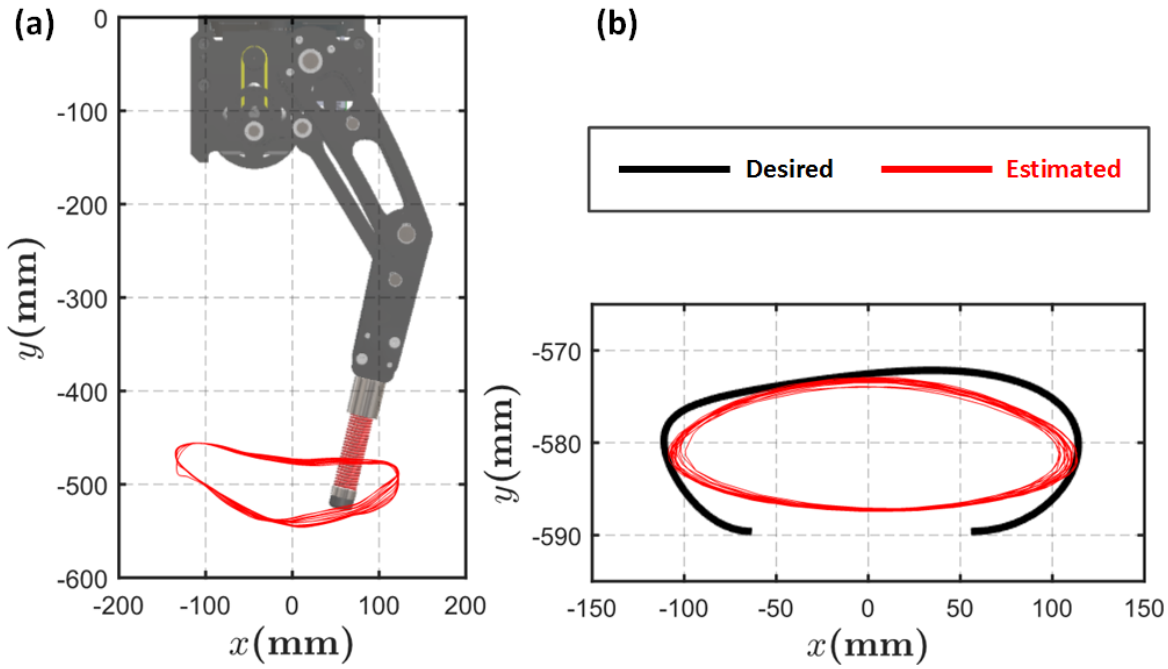

Figure 5.2: Illustrating the executed trajectory (red) by BOLT. (a)Depiction of the estimated trajectory at the speed of 1m/s. (b) Comparison of the designed trotting trajectory vs estimated trajectory at 3.2 m/s.

5.3 Open loop running

To test the performance of the robot, it was lowered to a configuration where in the leg makes point contact with the treadmill. The aim behind this experiment was to test the performance of the designed trajectory and to showcase the simplicity of the robot. It is observable in Figure 5.3 that BOLT completes a single cycle of motion in 300 ms at its top speed. It was able to achieve this simply on the basis of open loop control. The systems height was controlled throughout the experiment.

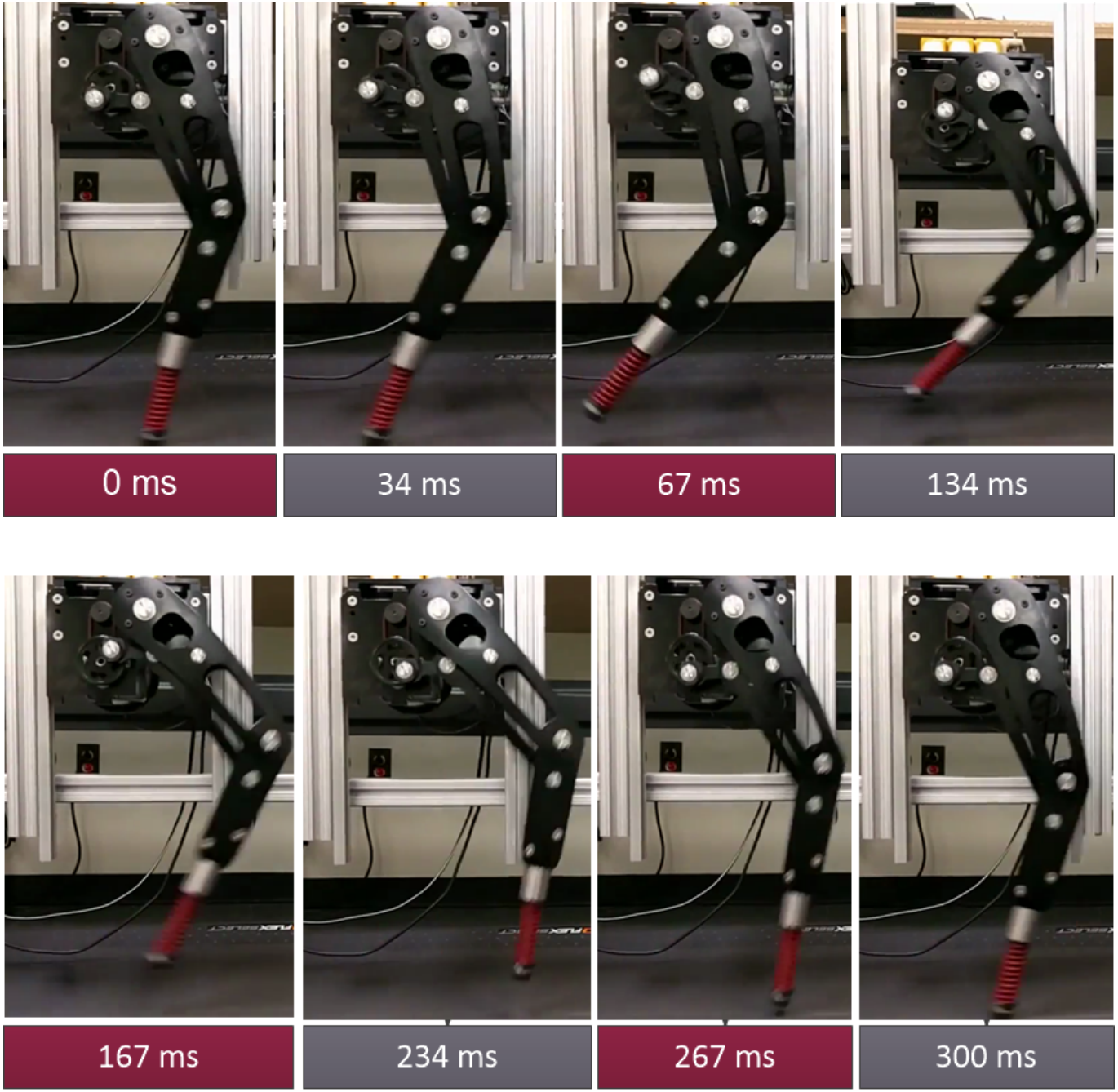

Figure 5.3: Timestamps illustrating one step cycle of the BOLT in open loop control

Chapter 6

Conclusion & Future Work

This chapter provides a conclusion to the thesis, it provides a brief summary of the current work and reviews the potential future work.

6.1 Summary

This thesis presented the design, analysis, prototype and integration of a novel single degree of freedom mechanism for dynamic locomotive gaits. The proposed design's novelty lies in the topological arrangement of the six bar mechanism. With this arrangement it proved its ability to trace a trajectory that is smooth and symmetrical in the stance phase.

With a comprehensive literature review we established the state of art robotic four legged machines and closely investigated there leg structures and capabilities. Armed with this knowledge we designed a six bar mechanism. A kinematic study was undertaken to evaluate the trajectory the foot traces. Although it is a closed curve, we observed that the angle of attack is steep and will result in the leg falling over. Hence, it was realized that a design optimization is required in order to end up with a working prototype. Prior to that

a sensitivity analysis was performed on two key link lengths to identify there effect on the trajectory. An ideal stride phase trajectory was also established to act as a reference.
With the established reference and a deeper knowledge of the mechanism, a multi-objective function is formulated with primary goals as minimal angle of attack and maximum stride length. The complete parametric optimization resulted in a topological configuration identified as Bio-inspired One DOF Leg for Trotting (BOLT). A simplified kinematic model is then formulated to generate the one to one mapping this mechanism is characterized by.
To then establish a mathematical description of the leg mechanism, a simplified dynamic model is developed making use of the singularly perturbed formulation. This simplification of the floating base closed kinematic chain dynamics are developed to aid in design of real-time controllers.
Finally, with the help of in-house sensor trajectory experiments are conducted to validate the optimized trajectory. Open loop running demonstrates the simplicity of the mechanism and its potential capabilities.

6.2 Future Work

While quadrupedal robots has seen significant improvements over time, the implementation complexity and the cost of production is a limiting factor for introducing such systems into the society yet. An alternative approach albeit restrictions imposed to the mobility can act as cheap and affordable for certain purposes. On the other hand such systems behave as perfect research platforms to investigate the result of decoupling locomotion and balance and has potential to deeply understand the extent of the coupling needed.
Owing to the highly satisfactory open loop running performance, immediate focus is to utilize the reduced order dynamics and establish high-level control for foot placement. This

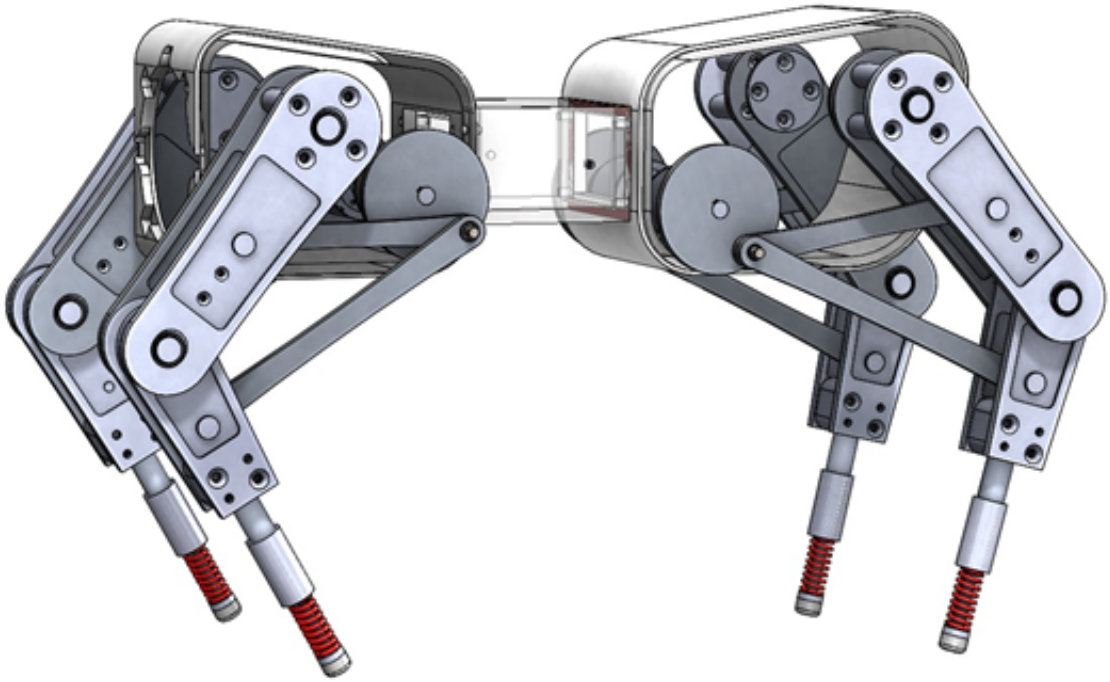

Figure 6.1: CAD rendering of the quadruped with the proposed leg mechanism

work will be then advanced to a full-size quadruped as in Figure 6.1. With the established simple dynamics, we aim to build high-level controllers for trotting with this machine. Also, extending into the near future the existing tails will be interfaced with BOLT quadruped. An attempt will be made to replicate the performance of existing multi DOF mechanism with the system shown inFigure 6.2

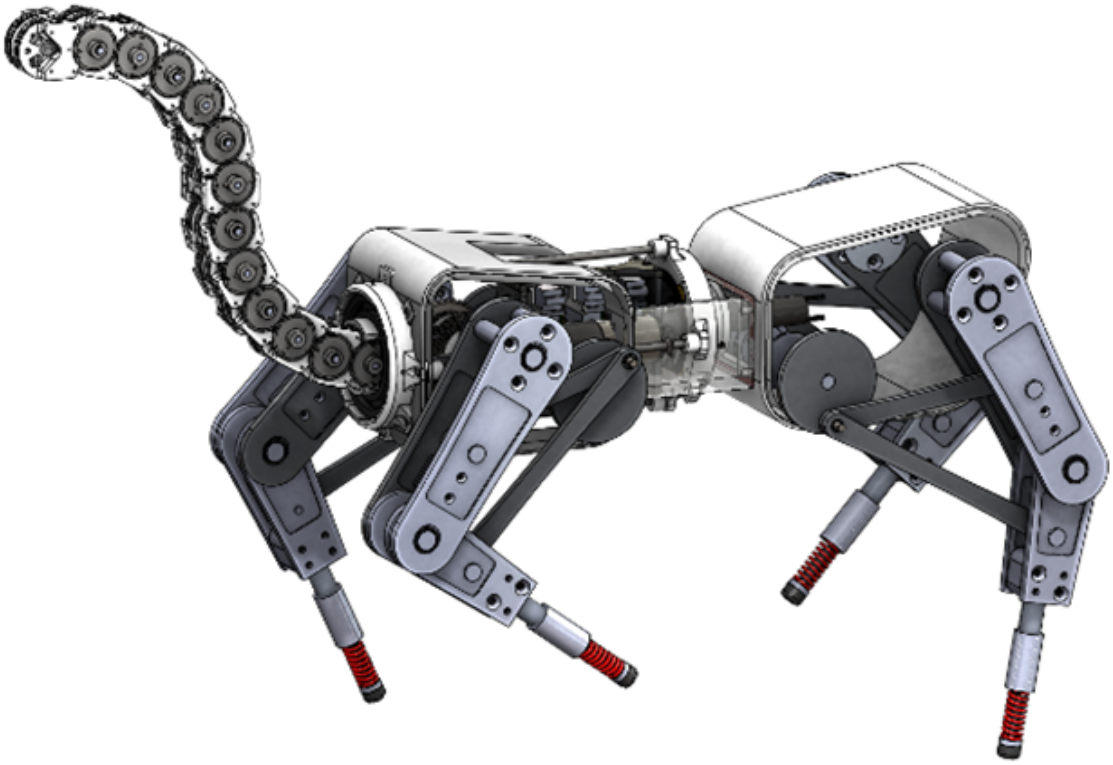

Figure 6.2: Fusion of the tail with the quadruped

Bibliography

[1] M. H. Raibert, "Trotting, pacing and bounding by a quadruped robot," *Journal of Biomechanics*, vol. 23, no. SUPPL. 1, pp. 79–98, 1990, ISSN: 00219290. DOI: 10.1016/0021-9290(90)90043-3.

[2] M. Hutter, C. Gehring, D. Jud, A. Lauber, C. D. Bellicoso, V. Tsounis, J. Hwangbo, P. Fankhauser, M. Bloesch, R. Diethelm, and S. Bachmann, "ANYmal - A Highly Mobile and Dynamic Quadrupedal Robot," *submitted to IEEE/RSJ Intenational Conference on Intelligent Robots and Systems (IROS)*, 2016. DOI: 10.3929/ethz-a-010686165.

[3] K. J. Waldron and R. B. McGhee, "The Adaptive Suspension Vehicle," *IEEE Control Systems Magazine*, vol. 6, no. 6, pp. 7–12, 1986, ISSN: 02721708. DOI: 10.1109/MCS.1986.1105145.

[4] R. J. Full, "Quantifying Dynamic Stability and Maneuverability in Legged Locomotion," *Integrative and Comparative Biology*, vol. 42, no. 1, pp. 149–157, 2002, ISSN: 1540-7063. DOI: 10.1093/icb/42.1.149. [Online]. Available: http://icb.oxfordjournals.org/cgi/doi/10.1093/icb/42.1.149.

[5] H. Murao, H. Tamaki, and S. Kitamura, "Walking pattern acquisition for quadruped robot by using modular reinforcement learning," *2001 IEEE International Conference on Systems, Man and Cybernetics. e-Systems and e-Man for Cybernetics in Cyberspace (Cat.No.01CH37236)*, vol. 3, no. 1, pp. 1402–1405, DOI: 10.1109/ICSMC.2001.973478.

[6] S.-M. Song and K. J. Waldron, *Machines That Walk*. MIT Press, 1988, p. 327, ISBN: 9780262515481.

[7] W. Saab and P. Ben-Tzvi, "Design and Analysis of a Robotic Modular Leg Mechanism," in *ASME International Design Engineering Technical Conferences & Computers and Information in Engineering Conference*, 2016, pp. 1–8.

[8] W. S. Rone and P. Ben-Tzvi, "Static Modeling of a Multi-Segment Serpentine Robotic Tail," *ASME International Design Engineering Technical Conference & Computers and Information in Engineering Conference*, pp. 1–9, 2015. DOI: 10.1115/DETC2015-46655.

[9] W. S. Rone and P. Ben-Tzvi, "Continuum Robotic Tail Loading Analysis for Mobile Robot Stabilization and Maneuvering," in *ASME International Design Engineering Technical Conferences & Computers and Information in Engineering Conference*, vol. 1, 2014, pp. 1–8.

[10] W. Rone and P. Ben-Tzvi, "Dynamic Modeling and Simulation of a Yaw-Angle Quadruped Maneuvering With a Planar Robotic Tail," *Journal of Dynamic Systems, Measurement, and Control*, vol. 138, no. 8, p. 084 502, 2016, ISSN: 0022-0434. DOI: 10.1115/1.4033103. [Online]. Available: http://dynamicsystems.asmedigitalcollection.asme.org/article.aspx?doi=10.1115/1.4033103.

[11] W. S. Rone and P. Ben-Tzvi, "Multi-Segment Continuum Robot Shape Estimation Using Passive Cable Displacements," *IEEE International Symposium on Robotic and Sensors Environments*, no. 1334227, pp. 21–23, 2013.

[12] R. M. Alexander, "The Gaits of Bipedal and Quadrupedal Animals," *The International Journal of Robotics Research*, vol. 3, no. 2, pp. 49–59, 1984, ISSN: 0278-3649. DOI: 10.1177/027836498400300205.

[13] A. Wang, S. Seok, A. Wang, D. Otten, and S. Kim, "Actuator Design for High Force Proprioceptive Control in Fast Legged Locomotion Actuator Design for High Force Proprioceptive Control in Fast Legged Locomotion," no. February 2016, pp. 1970–1975, 2012. DOI: 10.1109/IROS.2012.6386252.

[14] D. Jin Hyun, S. Seok, J. Lee, and S. Kim, "High speed trot-running: Implementation of a hierarchical controller using proprioceptive impedance control on the MIT Cheetah," *The International Journal of Robotics Research*, vol. 33, no. 11, pp. 1417–1445, 2014, ISSN: 0278-3649. DOI: 10.1177/0278364914532150.

[15] C. Semini, N. G. Tsagarakis, E. Guglielmino, M. Focchi, F. Cannella, and D. G. Caldwell, "Design of HyQ - a hydraulically and electrically actuated quadruped robot," *Proceedings of the Institution of Mechanical Engineers, Part I: Journal of Systems and Control Engineering*, vol. 225, no. 6, pp. 831–849, 2011, ISSN: 0959-6518. DOI: 10.1177/0959651811402275.

[16] H. Khan, S. Kitano, M. Frigerio, M. Camurri, V. Barasuol, R. Featherstone, D. G. Caldwell, and C. Semini, "Development of the lightweight hydraulic quadruped robot - MiniHyQ," *IEEE Conference on Technologies for Practical Robot Applications, TePRA*, vol. 2015-Augus, 2015, ISSN: 23250534. DOI: 10.1109/TePRA.2015.7219671.

[17] U. Saranli, M. Buehler, and D. E. Koditschek, "RHex: A Simple and Highly Mobile Hexapod Robot," *The International Journal of Robotics Research*, vol. 20, no. July, pp. 616–631, 2001, ISSN: 0278-3649. DOI: 10.1177/02783640122067570.

[18] C. Tavolieri, E. Ottaviano, M. Ceccarelli, and A. Di Rienzo, "Analysis and Design of a 1-DOF Leg for Walking Machines," *15th International Workshop on Robotics in AlpeAdria-Danube Region, Balantonfured, CD Proceedings,*, 2006. [Online]. Available: http://conf.uni-obuda.hu/raad2006/Ottaviano.pdf.

[19] A. Ghassaei, P. P. Choi, and D. Whitaker, "The Design and Optimization of a Crank-Based Leg Mechanism," 2011.

[20] A. Seyfarth, H. Geyer, and H. Herr, "Swing-leg retraction: a simple control model for stable running," *The Journal of experimental biology*, vol. 206, no. Pt 15, pp. 2547–2555, 2003, ISSN: 0022-0949. DOI: 10.1242/jeb.00463.

[21] T. Boaventura, C. Semini, J. Buchli, M. Frigerio, M. Focchi, and D. G. Caldwell, "Dynamic torque control of a hydraulic quadruped robot," *2012 IEEE International Conference on Robotics and Automation*, pp. 1889–1894, 2012, ISSN: 1050-4729. DOI: 10.1109/ICRA.2012.6224628. [Online]. Available: http://ieeexplore.ieee.org/document/6224628/.

[22] M. Mistry, J. Nakanishi, and S. Schaal, "Task space control with prioritization for balance and locomotion," *IEEE International Conference on Intelligent Robots and Systems*, no. 5, pp. 331–338, 2007. DOI: 10.1109/IROS.2007.4399595.

[23] T. Horvat, K. Melo, and A. J. Ijspeert, "Model Predictive Control Based Framework for CoM Control of a Quadruped Robot," pp. 3372–3378, 2017.

[24] M. Hutter, C. D. Remy, M. A. Hoepflinger, and R. Siegwart, "Scarl ETH : Design and Control of a Planar Running Robot," pp. 2–7, 2011.

[25] F. Farshidian, E. Jelavić, A. W. Winkler, and J. Buchli, "Robust Whole-Body Motion Control of Legged Robots," in *IEEE/RSJ International Conference on Intelligent Robots and Systems (IROS)*, Vancouver, BC, Canada, 2017, pp. 4589–4596, ISBN: 9781538626818. arXiv: 1703.02326. [Online]. Available: http://arxiv.org/abs/1703.02326.

[26] A. Del Prete and N. Mansard, "Robustness to Joint-Torque-Tracking Errors in Task-Space Inverse Dynamics," *IEEE Transactions on Robotics*, vol. 32, no. 5, pp. 1091–1105, 2016, ISSN: 15523098. DOI: 10.1109/TRO.2016.2593027.

[27] O Becker, I Pietsch, and J Hesselbach, "Robust task-space control of hydraulic robots," *Robotics and Automation, ...*, pp. 4360–4365, 2003, ISSN: 10504729. DOI: 10.1109/ROBOT.2003.1242275. [Online]. Available: http://ieeexplore.ieee.org/xpls/abs{_}all.jsp?arnumber=1242275.

[28] I. Poulakakis, J. A. Smith, and M. Buehler, "Modeling and Experiments of Untethered Quadrupedal Running with a Bounding Gait: The Scout II Robot," *The International Journal of Robotics Research*, vol. 24, no. 4, pp. 239–256, 2005, ISSN: 0278-3649. DOI: 10.1177/0278364904050917. [Online]. Available: http://journals.sagepub.com/doi/10.1177/0278364904050917.

[29] V. Kamidi, W. Saab, and P. Ben-Tzvi, "Design And Analysis of a Novel Planar Robotic Leg For High-Speed Locomotion," in *IEEE/RSJ International Conference on Intelligent Robots and Systems*, Vancouver, Canada, 2017, pp. 6343–6348, ISBN: 9781538626818.

[30] H. Geyer, A. Seyfarth, and R. Blickhan, "Spring-mass running: Simple approximate solution and application to gait stability," *Journal of Theoretical Biology*, vol. 232, no. 3, pp. 315–328, 2005, ISSN: 00225193. DOI: 10.1016/j.jtbi.2004.08.015.

[31] E. Haug, "Intermediate Dynamics," in, Prentice Hall College Div, 1991, pp 48–108.

[32] D. J. Hyun, J. Lee, S. Park, and S. Kim, "Implementation of trot-to-gallop transition and subsequent gallop on the MIT Cheetah I," *Int. J. Robot. Res.*, pp. 1–24, 2016, ISSN: 0278-3649. DOI: 10.1177/0278364916640102.

[33] D. P. Huttenlocher, G. A. Klanderman, and W. J. Rucklidge, "Comparing Images Using the Hausdorff Distance," *IEEE Transactions on Pattern Analysis and Machine Intelligence*, vol. 15, no. 9, pp. 850–863, 1993, ISSN: 01628828. DOI: 10.1109/34.232073.

[34] S. Niwattanakul, J. Singthongchai, E. Naenudorn, and S. Wanapu, "Using of Jaccard Coefficient for Keywords Similarity," *International MultiConference of Engineers and Computer Scientists*, vol. I, pp. 380–384, 2013, ISSN: 20780958. DOI: ISBN978-988-19251-8-3.

[35] M. W. Spong, S. Hutchinson, and M. Vidyasagar, *Robot modeling and control*, First, 6. John Wiley & Sons, Inc., 2006, vol. 26, pp. 113–115, ISBN: 0471649902. DOI: 10.1109/MCS.2006.252815.

[36] K. Brenan, S. Campbell, and L. Petzold, *Numerical Solution of Initial-Value Problems in Differential-Algebraic Equations*. Society for Industrial and Applied Mathematics, 1995. DOI: 10.1137/1.9781611971224. [Online]. Available: http://epubs.siam.org/doi/abs/10.1137/1.9781611971224.

[37] L. R. Petzold, "Numerical solution of differential-algebraic equations in mechanical systems simulation," *Physica D: Nonlinear Phenomena*, vol. 60, no. 1-4, pp. 269–279, 1992, ISSN: 01672789. DOI: 10.1016/0167-2789(92)90243-G.

[38] H. Krishnan and N. H. Mcclamroch, "Tracking in nonlinear differential-algebraic control systems with applications to constrained robot systems," *Automatica*, vol. 30, no. 12, pp. 1885–1897, 1994, ISSN: 00051098. DOI: 10.1016/0005-1098(94)90049-3.

[39] F. Ghorbel and O. Chetelat, "A Reduced Model for Constrained Rigid Bodies," in *Proc. of the IFAC Symposium on Robot Control SYROCO'94*, Capri, Italy, September 19-21, 1994, pp. 57–62.

[40] C. W. Gear, B. Leimkuhler, and G. K. Gupta, "Automatic integration of Euler-Lagrange equations with constraints," *Journal of Computational and Applied Mathematics*, vol. 12-13, no. C, pp. 77–90, 1985, ISSN: 03770427. DOI: 10.1016/0377-0427(85)90008-1.

[41] J. Baumgarte, "Stabilization of constraints and integrals of motion in dynamical systems," *Computer Methods in Applied Mechanics and Engineering*, vol. 1, no. 1, pp. 1–16, 1972, ISSN: 00457825. DOI: 10.1016/0045-7825(72)90018-7.

[42] U. M. Ascher, H. Chin, L. R. Petzold, and S. Reich, "Stabilization of Constrained Mechanical Systems with DAEs and Invariant Manifolds," *Mechanics of Structures and Machines*, vol. 23, no. 2, pp. 135–157, 1995, ISSN: 08905452. DOI: 10.1080/08905459508905232.

[43] Z. Wang and F. H. Ghorbel, "Control of Closed Kinematic Chains : A Comparative Study," in *Proceedings of the 2006 American Control Conference Minneapolis,*, Minneapolis, Minnesota, USA, 2006, pp. 2498–2503, ISBN: 1424402107. DOI: 10.1109/ACC.2006.1656597.

[44] X. Yun and N. Sarkar, "Unified formulation of robotic systems with holonomic and nonholonomic constraints," *IEEE Transactions on Robotics and Automation*, vol. 14, no. 4, pp. 640–650, 1998, ISSN: 1042296X. DOI: 10.1109/70.704238.

[45] F. H. Ghorbel, O. Chételat, R. Gunawardana, and R. Longchamp, "Modeling and set point control of closed-chain mechanisms: Theory and experiment," *IEEE Transactions on Control Systems Technology*, vol. 8, no. 5, pp. 801–815, 2000, ISSN: 10636536. DOI: 10.1109/87.865853.

[46] J. Wittenburg, *Dynamics of Multibody Systems*, Second. Springer.

[47] J. B. Dabney, F. H. Ghorbel, and Z. Wang, "Modeling closed kinematic chains via singular perturbations," *Proceedings of the American Control Conference*, vol. 5, pp. 4104–4110, 2002, ISSN: 07431619. DOI: 10.1109/ACC.2002.1024573.

[48] A. Kumar and P. Ben-Tzvi, "Spatial Object Tracking System Based on Linear Optical Sensor Arrays," *IEEE Sensors Journal*, vol. 16, no. 22, pp. 7933–7940, 2016, ISSN: 1530437X. DOI: 10.1109/JSEN.2016.2607120.

Appendix A

Floating Base EOM utilizing SPF

Refer to Figure 4.1 and Figure 4.2 for the notation used in deriving the EOMs of BOLT. First, the equations of motion are derived in the dependent co-ordinates and then are reduced to the independent co-ordinates using the Lagrangian formulation. Finally through the use of singularly perturbed formulation a complete solution is obtained.

The Kinetic energy, T is given by:

$$T = 0.5(I_1\dot{\phi}^2 + I_2\dot{\phi}^2 + I_3\dot{\phi}^2 + I_1\dot{q_1}^2 + I_2\dot{q_1}^2 + I_2\dot{q_2}^2 + I_3\dot{q_3}^2 + I\dot{\phi}^2 + m\dot{x}^2 + m_1\dot{x}^2 + m_2\dot{x}^2 + m_3\dot{x}^2 ..$$
$$+ m\dot{y}^2 + m_1\dot{y}^2 + m_2\dot{y}^2 + m_3\dot{y}^2 + \dot{\phi}^2 l_1^2 m_2 + \dot{q_1}^2 l_1^2 m_2 + \dot{\phi}^2 l_{cm,2}^2 m_2 + \dot{\phi}^2 l_{cm,3}^2 m_3 + \dot{q_1}^2 l_{cm,2}^2 m_2 + ..$$
$$\dot{q_2}^2 l_{cm,2}^2 m_2 + \dot{q_3}^2 l_{cm,3}^2 m_3 + \dot{\phi}^2 l_h^2 m_1 + \dot{\phi}^2 l_h^2 m_2 + I_1\dot{\phi}\dot{q_1} + I_2\dot{\phi}\dot{q_1} + I_2\dot{\phi}\dot{q_2} + I_3\dot{\phi}\dot{q_3} + I_2\dot{q_1}\dot{q_2} + \dot{\phi}\dot{q_1} l_1^2 m_2 + .$$
$$+ \dot{\phi}\dot{q_1} l_{cm,2}^2 m_2 + \dot{\phi}\dot{q_2} l_{cm,2}^2 m_2 + \dot{\phi}\dot{q_3} l_{cm,3}^2 m_3 + \dot{q_1}\dot{q_2} l_{cm,2}^2 m_2 + \dot{\phi}^2 l_{cm,2} l_h m_2 cos(q_1 + q_2) + ..$$
$$\dot{\phi}\dot{x} l_{cm,2} m_2 cos(\phi + q_1 + q_2) + \dot{q_1}\dot{x} l_{cm,2} m_2 cos(\phi + q_1 + q_2) + \dot{q_2}\dot{x} l_{cm,2} m_2 cos(\phi + q_1 + q_2) + ..$$
$$\dot{\phi}\dot{y} l_{cm,2} m_2 sin(\phi + q_1 + q_2) + \dot{q_1}\dot{y} l_{cm,2} m_2 sin(\phi + q_1 + q_2) + \dot{q_2}\dot{y} l_{cm,2} m_2 sin(\phi + q_1 + q_2) + ..$$
$$\dot{\phi}^2 l_1 l_{cm,2} m_2 cos(q_2) + \dot{q_1}^2 l_1 l_{cm,2} m_2 cos(q_2) + \dot{\phi}^2 l_1 l_h m_2 cos(q_1) + \dot{\phi}\dot{x} l_1 m_2 cos(\phi + q_1) + ..$$
$$\dot{q_1}\dot{x} l_1 m_2 cos(\phi + q_1) + \dot{q_3}\dot{x} l_{cm,3} m_3 cos(\phi + q_3) + \dot{q_3}\dot{x} l_{cm_3} m_3 cos(\phi + q_3) + \dot{\phi}\dot{y} l_1 m_2 sin(\phi + q_1) + ..$$
$$\dot{q_1}\dot{y} l_1 m_2 sin(\phi + q_1) + \dot{\phi}\dot{y} l_{cm_3} m_3 sin(\phi + q_3) + \dot{q_3}\dot{y} l_{cm_3} m_3 sin(\phi + q_3) + \dot{\phi}\dot{x} l_h m_1 cos(\phi) + ..$$
$$\dot{\phi}\dot{x} l_h m_2 cos(\phi) + \dot{\phi}\dot{y} l_h m_1 sin(\phi) + \dot{\phi}\dot{y} l_h m_2 sin(\phi) + \dot{\phi}\dot{q_1} l_{cm,2} l_h m_2 cos(q_1 + q_2) + ..$$
$$\dot{\phi}\dot{q_2} l_{cm,2} l_h m_2 cos(q_1 + q_2) + 2\dot{\phi}\dot{q_1} l_1 l_{cm,2} m_2 cos(q_2) + \dot{\phi}\dot{q_2} l_1 l_{cm,2} m_2 cos(q_2) + \dot{q_1}\dot{q_2} l_1 l_{cm,2} m_2 cos(q_2) + ..$$
$$\dot{\phi}\dot{q_1} l_1 l_h m_2 cos(q_1))$$
(A.1)

Likewise, the potential energy V is given as:

$$V = -g(l_h m_1 cos(\phi) - m_1 y - m_2 y - m_3 y - my + l_h m_2 cos(\phi) + l_{cm,2} m_2 cos(\phi + q_1 + q_2) + ..$$
$$l_2 m_2 cos(\phi + q_1) + l_{cm,3} m_3 cos(\phi + q_3))$$
(A.2)

The equation of motion during swing phase in dependent generalized coordinates is given by:

$$M(q_d)\ddot{q}_d + C(q_d, \dot{q}_d)\dot{q}_d + g(q_d) = Bu$$

$$M_{1,1}(q_d) = m + m_1 + m_2 + m_3$$

$$M_{1,2}(q_d) = 0$$

$$M_{1,3}(q_d) = l_h m_1 \cos(\phi) \; + l_h m_2 \cos(\phi)$$

$$+ l_{cm,2} m_2 \cos(\phi + q_1 + q_2)$$

$$+ l_1 m_2 \cos(\phi + q_1) \; + \; l_{cm,3} m_3 \cos(\phi + q_3)$$

$$M_{1,4}(q_d) = l_{cm,2} m_2 \cos(\phi + q_1 + q_2) \; + l_1 m_2 \cos(\phi + q_1)$$

$$M_{1,5}(q_d) = l_{cm,2} m_2 \cos(\phi + q_1 + q_2)$$

$$M_{1,6}(q_d) = l_{cm,3} m_3 \cos(\phi + q_3)$$

$$M_{2,1}(q_d) = 0$$

$$M_{2,2}(q_d) = m + m_1 + m_2 + m_3$$

$$M_{2,3}(q_d) = l_h m_1 \sin(\phi) + l_h m_2 \sin(\phi)$$

$$+ l_{cm,2} m_2 \sin(\phi + q_1 + q_2)$$

$$+ l_1 m_2 \sin(\phi + q_1) \; + \; l_{cm,3} m_3 \sin(\phi + q_3)$$

$$M_{2,4}(q_d) = l_{cm,2} m_2 \sin(\phi + q_1 + q_2)$$

$$+ l_1 m_2 \sin(\phi + q_1)$$

$$M_{2,5}(q_d) = l_{cm,2} m_2 \sin(\phi + q_1 + q_2)$$

$$M_{2,6}\left(q_d\right) = l_{cm,3}m_3\sin\left(\phi + q_3\right)$$

$$M_{3,1}\left(q_d\right) = l_h m_1\cos\left(\phi\right) \ + l_h m_2\cos\left(\phi\right)$$

$$+l_{cm,2}m_2\cos\left(\phi + q_1 + q_2\right)$$

$$+l_1 m_2\cos\left(\phi + q_1\right) \ + \ l_{cm,3}m_3\cos(\phi + q_3)$$

$$M_{3,2}\left(q_d\right) = l_h m_1\sin\left(\phi\right) \ + l_h m_2\sin\left(\phi\right)$$

$$+l_{cm,2}m_2\sin\left(\phi + q_1 + q_2\right)$$

$$+l_1 m_2\sin\left(\phi + q_1\right) \ + l_{cm,3}m_3\sin\left(\phi + q_3\right)$$

$$M_{3,3}\left(q_d\right) = I_1 + I_2 + I_3 + I + l_1^2 m_2$$

$$+l_{cm,2}^2 m_2 + l_{cm,3}^2 m_3 + l_h^2 \ m_1$$

$$+l_h^2 m_2 + 2l_{cm.2}l_h m_2\cos\left(q_1 + q_2\right)$$

$$+2 \ l_1\mathrm{l}_{\mathrm{cm},2}\mathrm{m}_2\cos(q_2) \ + 2 \ l_1\mathrm{l}_{\mathrm{h}}\mathrm{m}_2\cos(q_1)$$

$$M_{3,4}\left(q_d\right) = m_2 l_1^2 + 2 \ m_2\cos\left(q_2\right) \ l_1 l_{cm,2}$$

$$+l_h m_2\cos\left(q_1\right) \ l_1 + m_2 l_{cm,2}^2$$

$$+l_h m_2\cos\left(q_1 + q_2\right) \ l_{cm,2} + I_1 + I_2$$

$$M_{3,5}\left(q_d\right) = I_2 + l_{cm,2}^2 m_2 + l_{cm,2}l_h m_2\cos\left(q_1 + q_2\right)$$

$$+l_1 l_{cm,2}m_2\cos(q_2)$$

$$M_{3,6}\left(q_d\right) = m_3 l_{cm,3}^2 + I_3$$

$$M_{4,1}\left(q_d\right) = l_{cm,2}m_2\cos\left(\phi + q_1 + q_2\right)$$

$$+l_1 m_2 \cos(\phi + q_1)$$

$$M_{4,2}\left(q_d\right) = l_{cm,2} m_2 \sin\left(\phi + q_1 + q_2\right)$$

$$+l_1 m_2 \sin(\phi + q_1)$$

$$M_{4,3}\left(q_d\right) = m_2 l_1^2 + 2\ m_2 \cos\left(q_2\right)\ l_1 l_{cm,2}$$

$$+l_h m_2 \cos\left(q_1\right)\ l_1\ + m_2 \mathrm{l}_{\mathrm{cm},2}^2 + \mathrm{l_h} m_2 \cos\left(q_1 + q_2\right)$$

$$l_{cm,2} + I_1 + I_2$$

$$M_{4,4}\left(q_d\right) = m_2 l_1^2 + 2\ m_2 \cos\left(q_2\right)\ l_1 l_{cm,2}\ + m_2 l_{cm,2}^2$$

$$+\ I_1 + I_2$$

$$M_{4,5}\left(q_d\right) = m_2 l_{cm,2}^2 + l_1 m_2 \cos\left(q_2\right)\ l_{cm,2} + I_2$$

$$M_{4,6}\left(q_d\right) = 0$$

$$M_{5,1}\left(q_d\right) = l_{cm,2} m_2 \cos(\phi + q_1 + q_2)$$

$$M_{5,2}\left(q_d\right) = l_{cm,2} m_2 \sin(\phi + q_1 + q_2)$$

$$M_{5,3}\left(q_d\right) = I_2 + l_{cm,2}^2 m_2 + l_{cm,2} l_h m_2 \cos\left(q_1 + q_2\right)$$

$$+\ l_1 l_{cm,2} m_2 \cos(q_2)$$

$$M_{5,4}\left(q_d\right) = m_2 l_{cm,2}^2 + l_1 m_2 \cos\left(q_2\right)\ l_{cm,2} + I_2$$

$$M_{5,5}\left(q_d\right) = m_2 l_{cm,2}^2 + I_2$$

$$M_{5,6}\left(q_d\right) = 0$$

$$M_{6,1}\left(q_d\right) = l_{cm,3} m_3 \cos\left(\phi + q_3\right)$$

$$M_{6,2}\left(q_d\right) = l_{cm,3} m_3 \ \sin(\phi + q_3)$$

$$M_{6,3}\left(q_d\right) = m_3 l_{cm,3}^2 + I_3$$

$$M_{6,4}\left(q_d\right) = 0$$

$$M_{6,5}\left(q_d\right) = 0$$

$$M_{6,6}\left(q_d\right) = m_3 l_{cm,3}^2 \ + I_3$$

$$C_{1,1}\left(q_d\right) = 0$$

$$C_{1,2}\left(q_d\right) = 0$$

$$C_{1,3}\left(q_d\right) = -\dot{q}(l_{cm,2} m_2 \sin\left(\phi + q_1 + q_2\right)$$

$$+ l_1 m_2 \sin(\phi + q_1))$$

$$-\dot{\phi}(l_h m_1 \sin\left(\phi\right) \ + l_h m_2 \sin\left(\phi\right)$$

$$+ l_{cm,2} m_2 \sin\left(\phi + q_1 + q_2\right)$$

$$+ l_1 m_2 \sin\left(\phi + q_1\right) \ + l_{cm,3} m_3 \sin(\phi + q_3))$$

$$-\dot{q_3} l_{cm,3} m_3 \sin\left(\phi + q_3\right)$$

$$-\dot{q_2} l_{cm,2} m_2 \sin(\phi + q_1 + q_2)$$

$$C_{1,4}\left(q_d\right) = -\dot{\phi}(l_{cm,2} m_2 \sin\left(\phi + q_1 + q_2\right)$$

$$+ l_1 m_2 \sin(\phi + q_1))$$

$$-\dot{q_1}(l_{cm,2}m_2\sin(\phi+q_1+q_2)$$

$$+l_1m_2\sin(\phi+q_1))$$

$$-\dot{q_2}l_{cm,2}m_2\sin(\phi+q_1+q_2)$$

$$C_{1,5}(q_d) = -l_{cm,2}m_2\sin(\phi+q_1+q_2)(\dot{\phi}+\dot{q_1}+\dot{q_2})$$

$$C_{1,6}(q_d) = -l_{cm,3}m_3\sin(\phi+q_3)(\dot{\phi}+\dot{q_3})$$

$$C_{2,1}(q_d) = 0$$

$$C_{2,2}(q_d) = 0$$

$$C_{2,3}(q_d) = \dot{\phi}(l_hm_1\cos(\phi) \ + l_hm_2\cos(\phi)$$

$$+l_{cm,2}m_2\cos(\phi+q_1+q_2)$$

$$+l_1m_2\cos(\phi+q_1) \ + l_{cm,3}m_3\cos(\phi+q_3))$$

$$+\dot{q_1}(l_{cm,2}m_2\cos(\phi+q_1+q_2)$$

$$+l_1m_2\cos(\phi+q_1)) + \dot{q_3} \ l_{cm,3}m_3\cos(\phi+q_3)$$

$$+\dot{q_2}l_{cm,2}m_2\cos(\phi+q_1+q_2)$$

$$C_{2,4}(q_d) = -\dot{\phi}(l_{cm,2}m_2\cos(\phi+q_1+q_2)$$

$$+l_1m_2\cos(\phi+q_1))$$

$$-\dot{q_1}(l_{cm,2}m_2\cos(\phi+q_1+q_2)$$

$$+l_1m_2\cos(\phi+q_1))$$

$$-\dot{q_2}l_{cm,2}m_2\cos(\phi+q_1+q_2)$$

$$C_{2,5}\left(q_d\right) = l_{cm,2} m_2 \cos\left(\phi + q_1 + q_2\right)\ \left(\dot{\phi} + \dot{q_1} + \dot{q_2}\right)$$

$$C_{2,6}\left(q_d\right) = l_{cm,3} m_3 \cos\left(\phi + q_3\right)\ \left(\dot{\phi} + \dot{q_3}\right)$$

$$C_{3,1}\left(q_d\right) = 0$$

$$C_{3,2}\left(q_d\right) = 0$$

$$C_{3,3}\left(q_d\right) = -\dot{q_2}\left(l_{cm,2} l_h m_2 \sin\left(q_1 + q_2\right)\ \right)$$

$$+\ l_1 l_{cm,2} m_2 \sin\left(q_2\right))$$

$$-\dot{q_1}(l_{cm,2} l_h m_2 \sin\left(q_1 + q_2\right)$$

$$+ l_1 l_h m_2 \sin(q_1))$$

$$C_{3,4}\left(q_d\right) = -\dot{q_2}\left(l_{cm,2} l_h m_2 \sin\left(q_1 + q_2\right)\ \right)$$

$$+\ l_1 l_{cm,2} m_2 \sin\left(q_2\right))$$

$$-\dot{\phi}(l_{cm,2} l_h m_2 \sin\left(q_1 + q_2\right)$$

$$+ l_1 l_h m_2 \sin(q_1))$$

$$-\dot{q_1}(l_{cm,2} l_h m_2 \sin\left(q_1 + q_2\right)\ + l_1 l_h m_2 \sin(q_1))$$

$$C_{3,5}\left(q_d\right) = -l_{cm,2} m_2 (l_h \sin\left(q_1 + q_2\right)\ + l_1 \sin(q_2))$$

$$*(\dot{\phi} + \dot{q_1} + \dot{q_2})$$

$$C_{3,6}\left(q_d\right) = 0$$

$$C_{4,1}\left(q_d\right) = 0$$

$$C_{4,2}\left(q_d\right) = 0$$

$$C_{4,3}\left(q_d\right) = \dot{\phi}\left(l_{cm,2} l_h m_2 \sin\left(q_1 + q_2\right) \; + l_1 l_h m_2 \sin\left(q_1\right) \; \right)$$

$$-\dot{q_2} l_1 l_{cm,2} m_2 \sin(q_2)$$

$$C_{4,4}\left(q_d\right) = -\dot{q_2} l_1 l_{cm,2} m_2 \sin(q_2)$$

$$C_{4,5}\left(q_d\right) = \; -l_1 l_{cm,2} m_2 \sin(q_2)(\dot{\phi} + \dot{q_1} + \dot{q_2})$$

$$C_{4,6}\left(q_d\right) = 0$$

$$C_{5,1}\left(q_d\right) = 0$$

$$C_{5,2}\left(q_d\right) = 0$$

$$C_{5,3}\left(q_d\right) = \dot{\phi}\left(l_{cm,2} l_h m_2 \sin\left(q_1 + q_2\right) \; + l_1 l_{cm,2} m_2 \sin\left(q_2\right) \; \right)$$

$$+ \; \dot{q_1} l_1 l_{cm,2} m_2 \sin(q_2)$$

$$C_{5,4}\left(q_d\right) = l_1 l_{cm,2} m_2 \sin(q_2)(\dot{\phi} + \dot{q_1})$$

$$C_{5,5}\left(q_d\right) = 0$$

$$C_{5,6}\left(q_d\right) = 0$$

$$C_{6,1}\left(q_d\right) = 0$$

$$C_{6,2}\left(q_d\right) = 0$$

$$C_{6,3}\left(q_d\right) = 0$$

$$C_{6,4}\left(q_d\right) = 0$$

$$C_{6,5}\left(q_d\right) = 0$$

$$C_{6,6}\left(q_d\right) = 0$$

$$G_1\left(q_d\right) = 0$$

$$G_2\left(q_d\right) = g(m + m_1 + m_2 + m_3)$$

$$G_3\left(q_d\right) = g(l_h m_1 \sin\left(\phi\right) \ + l_h m_2 \sin\left(\phi\right)$$

$$+ l_{cm,2} m_2 \sin\left(\phi + q_1 + q_2\right) + l_1 m_2 \sin\left(\phi + q_1\right)$$

$$+ l_{cm,3} m_3 \sin(\phi + q_3))$$

$$G_4\left(q_d\right) = g m_2 (l_1 \sin(\phi + q_1) + l_{cm,2} \sin(\phi + q_1 + q_2))$$

$$G_5\left(q_d\right) = g l_{cm,2} m_2 \sin(\phi + q_1 + q_2)$$

$$G_6\left(q_d\right) = g l_{cm,3} \mathrm{m}_3 \sin(\phi + q_3)$$

Now Performing the matrix reduction using Equation 4.10; the M, C and G become a 4×4 matrix

$$M_{1,1}\left(q,\ z\right) = m + m_1 + m_2 + m_3$$

$$M_{1,2}\left(q, z\right) = 0$$

$$M_{1,3}\left(q, z\right) = l_h m_1 \cos\left(\phi\right) \ + l_h m_2 \cos\left(\phi\right)$$

$$+ l_{cm,2} m_2 \cos\left(\phi + q_1 + q_2\right)$$

$$+ l_1 m_2 \cos\left(\phi + q_1\right) \ + \ l_{cm,3} m_3 \cos(\phi + q_3)$$

$$M_{1,4}\left(q, z\right) = l_1 (l_2 m_3 \sin\left(\phi + q_2 + q_3\right) \ + l_{cm,2} m_2 \sin\left(\phi + q_2 + q_3\right)$$

$$+ l_2 m_2 \sin\left(\phi + q_2 + q_3\right)$$

$$+l_2 m_2 \sin(\phi + 2q_1 + q_2 - q_3)$$

$$-l_{cm,2} m_2 \sin(\phi + 2q_1 + q_2 - q_3)\ -l_2 m_2 \sin(\phi - q_2 + q_3)\ -l_2 m_3 \sin(\phi - q_2 + q_3))/(2l_2 \sin(q_1 + q_2 - q_3))$$

$$M_{2,1}(q_d) = 0$$

$$M_{2,2}(q_d) = m + m_1 + m_2 + m_3$$

$$M_{2,3}(q_d) = l_h m_1 \sin(\phi) + l_h m_2 \sin(\phi)$$

$$+l_{cm,2} m_2 \sin(\phi + q_1 + q_2)$$

$$+l_1 m_2 \sin(\phi + q_1)\ +\ l_{cm,3} m_3 \sin(\phi + q_3)$$

$$M_{2,4}(q, z) = l_1(l_2 m_3 \cos(\phi + q_2 + q_3)\ + l_{cm,2} m_2 \cos(\phi + q_2 + q_3)$$

$$+l_2 m_2 \cos(\phi + 2q_1 + q_2 - q_3)$$

$$-l_{cm,2} m_2 \cos(\phi + 2q_1 + q_2 - q_3)\ -l_2 m_2 \cos(\phi - q_2 + q_3)\ -l_2 m_3 \cos(\phi - q_2 + q_3))/(2l\_2 \sin(q_1 + q_2 - q_3))$$

$$M_{3,1}(q_d) = l_h m_1 \cos(\phi)\ + l_h m_2 \cos(\phi)$$

$$+l_{cm,2} m_2 \cos(\phi + q_1 + q_2)$$

$$+l_1 m_2 \cos(\phi + q_1)\ +\ l_{cm,3} m_3 \cos(\phi + q_3)$$

$$M_{3,2}(q_d) = l_h m_1 \sin(\phi)\ + l_h m_2 \sin(\phi)$$

$$+l_{cm,2} m_2 \sin(\phi + q_1 + q_2)$$

$$+l_1 m_2 \sin(\phi + q_1)\ + l_{cm,3} m_3 \sin(\phi + q_3)$$

$$M_{3,3}(q_d) = I_1 + I_2 + I_3 + I + l_1^2 m_2 + l_{cm,2}^2 m_2 + l_{cm,3}^2 m_3$$

$$+l_h^2\ m_1 + l_h^2 m_2 + 2l_{cm.2} l_h m_2 \cos(q_1 + q_2)$$

$$+2\ l_1 \mathrm{l}_{\mathrm{cm},2} \mathrm{m}_2 \mathrm{cos}(q_2)\ +2\ l_1 \mathrm{l}_{\mathrm{h}} \mathrm{m}_2 \mathrm{cos}(q_1)$$

$$M_{3,4}\left(q_d\right) = 2I_1 I_2 l_{cm,3} \mathrm{sin}\left(q_1+q_2-q_3\right)\ +2I_3 l_1 l_2 \mathrm{sin}\left(q_2\right)\ -2I_2 l_1 l_{cm,3} \mathrm{sin}\left(q_1-q_3\right)\ +l_{cm,3}^2 m_3$$

$$+2I_1 l_2 l_{cm,2}^2 m_3 \mathrm{sin}\left(q_2\right)\ -2l_1 l_{cm,2}^2 l_{cm,3} m_2 \mathrm{sin}\left(q_1-q_3\right)\ +2l_1^2 l_2 l_{cm,3} m_2 \mathrm{sin}\left(q_1+q_2-q_3\right)$$

$$-l_1^2 l_{cm,3} m_2 \mathrm{sin}\left(q_1+q_2-q_3\right)\ +l_1^2 l_{cm,2} l_{cm,3} m_2 \mathrm{sin}\left(q_2-q_1+q_3\right)\ +l_1 l_{cm,2} l_{cm,3} l_h m_2 \mathrm{sin}\left(q_2+q_3\right)$$

$$+\ l_1 l_2 l_{cm,2} l_{cm,3} m_2 \mathrm{sin}\left(q_1+2q_2-q_3\right)\ +l_1 l_2 l_{cm,3} l_h m_2 \mathrm{sin}\left(2q_1+q_2-q_3\right)$$

$$-l_1 l_{cm,2}\ l_{cm,3} l_h m_2 \mathrm{sin}(2q_1+q_2-q_3)$$

$$+l_1 l_2 l_{cm,2}\ l_{cm,3} m_2 \mathrm{sin}\left(q_1-q_3\right)\ +l_1 l_2 l_{cm,3} l_h m_2 \mathrm{sin}\left(q_2-q_3\right)\ /(2l_2 l_{cm,3} \mathrm{sin}(q_1+q_2-q_3))$$

$$M_{4,1}\left(q,z\right) = l_1(l_2 m_3 \mathrm{sin}\left(\phi+q_2+q_3\right)\ +l_{cm,2} m_2 \mathrm{sin}\left(\phi+q_2+q_3\right)$$

$$+l_2 m_2 \mathrm{sin}\left(\phi+q_2+q_3\right)$$

$$+l_2 m_2 \mathrm{sin}\left(\phi+2q_1+q_2-q_3\right)$$

$$-l_{cm,2} m_2 \mathrm{sin}\left(\phi+2q_1+q_2-q_3\right)\ -l_2 m_2 \mathrm{sin}\left(\phi-q_2+q_3\right)\ -l_2 m_3 \mathrm{sin}(\phi-q_2+q_3))/(2l_2 \mathrm{sin}(q_1+q_2-q_3))$$

$$M_{4,2}\left(q,z\right) = l_1(l_2 m_3 \mathrm{cos}\left(\phi+q_2+q_3\right)\ +l_{cm,2} m_2 \mathrm{cos}\left(\phi+q_2+q_3\right)$$

$$+l_2 m_2 \mathrm{cos}\left(\phi+2q_1+q_2-q_3\right)$$

$$-l_{cm,2} m_2 \mathrm{cos}\left(\phi+2q_1+q_2-q_3\right)\ -l_2 m_2 \mathrm{cos}\left(\phi-q_2+q_3\right)\ -l_2 m_3 \mathrm{cos}(\phi-q_2+q_3))/(2l\_2\ \mathrm{sin}(q_1+q_2-q_3))$$

$$M_{4,3}\left(q_d\right) = 2I_1 I_2 l_{cm,3} \mathrm{sin}\left(q_1+q_2-q_3\right)\ +2I_3 l_1 l_2 \mathrm{sin}\left(q_2\right)\ -2I_2 l_1 l_{cm,3} \mathrm{sin}\left(q_1-q_3\right)\ +l_{cm,3}^2 m_3$$

$$+2I_1 l_2 l_{cm,2}^2 m_3 \mathrm{sin}\left(q_2\right)\ -2l_1 l_{cm,2}^2 l_{cm,3} m_2 \mathrm{sin}\left(q_1-q_3\right)\ +2l_1^2 l_2 l_{cm,3} m_2 \mathrm{sin}\left(q_1+q_2-q_3\right)$$

$$-l_1^2 l_{cm,3} m_2 \mathrm{sin}\left(q_1+q_2-q_3\right)\ +l_1^2 l_{cm,2} l_{cm,3} m_2 \mathrm{sin}\left(q_2-q_1+q_3\right)$$

$$+l_1 l_{cm,2} l_{cm,3} l_h m_2 \mathrm{sin}\left(q_2+q_3\right) + l_1 l_2 l_{cm,2} l_{cm,3} m_2 \mathrm{sin}\left(q_1+2q_2-q_3\right) +l_1 l_2 l_{cm,3} l_h m_2 \mathrm{sin}\left(2q_1+q_2-q_3\right)$$

$$-l_1 l_{cm,2}\ l_{cm,3} l_h m_2 \sin(2q_1 + q_2 - q_3)\ + l_1 l_2 l_{cm,2}\ l_{cm,3} m_2 \sin(q_1 - q_3)$$

$$+ l_1 l_2 l_{cm,3} l_h m_2 \sin(q_2 - q_3)\ /(2 l_2 l_{cm,3} \sin(q_1 + q_2 - q_3))$$

$$M_{4,4}(q,z) = -I_3 l_1^2 l_2^2 + I_1 l_2^2 l_{cm,3}^2 + I_2 l_1^2 l_{cm,3}^2 + l_1^2 l_2^2 l_{cm,3}^2 2m_2 + l_1^2 l_2^2 l_{cm,3}^2 2m_3 + l_1^2 l_{cm,2}^2 2 l_{cm,3}^2 m_2 - I_3 l_1^2 l_2^2 \cos(2q_2)$$

$$-I_1 l_2^2 l_{cm,3}^2 \cos(2q_1 + 2q_2 - 2q_3)\ - I_2 l_1^2 l_{cm,3}^2 \cos(2q_1 - 2q_3)\ - l_1^2 l_2 l_{cm,2} l_{cm,3}^2 m_2 - l_1^2 l_2^2 l_{cm,3}^2 m_3 \cos(2q_2)$$

$$-l_1^2 l_2^2 l_{cm,3}^2 m_2 \cos(2q_1 + 2q_2 - 2q_3)\ - l_1^2 l_{cm,2}^2 l_{cm,3}^2 m_2 \cos(2q_1 - 2q_3)\ - l_1^2 l_2 l_{cm,2} l_{cm,3}^2 m_2 \cos(2q_2)$$

$$+ l_1^2 l_2 l_{cm,2} l_{cm,3}^2 m_2 \cos(2q_1 + 2q_2 - 2q_3)$$

$$+ l_1^2 l_2 l_{cm,2} l_{cm,3}^2 m_2 \cos(2q_1 - 2q_3) / (l_2^2 l_{cm,3}^2 (\cos(2q_1 + 2q_2 - 2q_3)\ - 1)$$

$$G_1(q,z) = 0$$

$$G_2(q,z) = g(m + m_1 + m_2 + m_3)$$

$$G_3(q,z) = g(l_h m_1 \sin(\phi)\ + l_h m_2 \sin(\phi)$$

$$+ l_{cm,2} m_2 \sin(\phi + q_1 + q_2) + l_1 m_2 \sin(\phi + q_1)$$

$$+ l_{cm,3} m_3 \sin(\phi + q_3))$$

$$G_4(q,z) = g l_1 (l_2 m_3 \cos(\phi + q_2 + q_3)\ + l_{cm,2} m_2 \cos(\phi + q_2 + q_3)$$

$$+ l_2 m_2 \cos(\phi + 2q_1 + q_2 - q_3) + l_{cm,2} m_2 \cos(\phi + 2q_1 + q_2 - q_3)$$

$$-l_2 m_2 \cos(\phi + 2q_1 + q_2 - q_3)\ - l_2 m_2 \cos(\phi - q_2 + q_3)\ - l_2 m_3 \cos(\phi - q_2 + q_3)) / (2 l_2 \sin(q_1 + q_2 - q_3))$$